JACS
JOURNAL OF THE AMERICAN CHEMICAL SOCIETY
pubs.acs.org/JACS
Article

Secondary Ion Mass Spectrometry of Single Giant Unilamellar Vesicles Reveals Compositional Variability

Dashiel S. Grusky, Ahanjit Bhattacharya, and Steven G. Boxer*

Cite This: J. Am. Chem. Soc. 2023, 145, 27521−27530
Read Online

ABSTRACT: Giant unilamellar vesicles (GUVs) are a widely used model system to interrogate lipid phase behavior, study biomembrane mechanics, reconstitute membrane proteins, and provide a chassis for synthetic cells. It is generally assumed that the composition of individual GUVs is the same as the nominal stock composition; however, there may be significant compositional variability between individual GUVs. Although this compositional heterogeneity likely impacts phase behavior, the function and incorporation of membrane proteins, and the encapsulation of biochemical reactions, it has yet to be directly quantified. To assess heterogeneity, we use secondary ion mass spectrometry (SIMS) to probe the composition of individual GUVs using non-perturbing isotopic labels. Both ^{13}C- and ^{2}H-labeled lipids are incorporated into a ternary mixture, which is then used to produce GUVs via gentle hydration or electroformation. Simultaneous detection of seven different ion species via SIMS allows for the concentration of ^{13}C- and ^{2}H-labeled lipids in single GUVs to be quantified using calibration curves, which correlate ion intensity to composition. Additionally, the relative concentration of ^{13}C- and ^{2}H-labeled lipids is assessed for each GUV via the ion ratio $^{2}H^{-}/^{13}C^{-}$, which is highly sensitive to compositional differences between individual GUVs and circumvents the need for calibration by using standards. Both quantification methods suggest that gentle hydration produces GUVs with greater compositional variability than those formed by electroformation. However, both gentle hydration and electroformation display standard deviations in composition (n = 30 GUVs) on the order of 1−4 mol %, consistent with variability seen in previous indirect measurements.

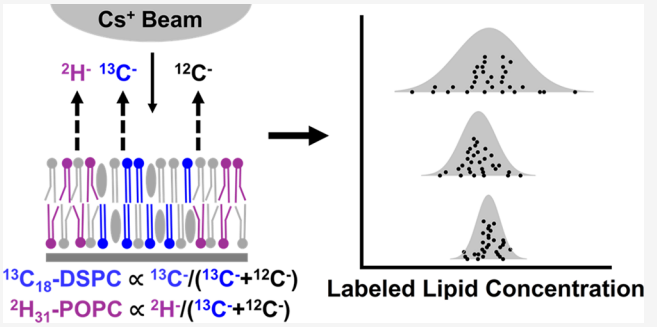

INTRODUCTION

Giant unilamellar vesicles (GUVs) are a commonly used model system to probe lipid phase behavior,[1−4] membrane−protein interactions,[5−10] and to encapsulate cellular machinery.[11−14] GUVs are attractive model systems not only due to their large size (typically 10−20 μm in diameter), which allows for convenient imaging via optical microscopy[15−21] but also due to their ease of production.

GUVs are commonly produced by either gentle hydration or electroformation. Although both methods start with a lipid mixture dried as a film, for gentle hydration the film is dried onto glass, while for electroformation the film is dried onto either platinum electrodes or indium tin oxide slides.[22] Films used for gentle hydration are heated above the melting point of the lipid mixture in the presence of either heated aqueous or heated sucrose solution.[23−25] The temperature is maintained above the melting point of the lipid mixture for the duration of GUV formation. Films used for electroformation are also rehydrated, typically at low ionic strength, before alternating current is applied to the film, which assists in the formation of GUVs.[26−28] This process is similarly conducted at temperatures above the melting point of the lipid mixture.

Despite their widespread use, there is some evidence pointing to potential issues with GUVs as model systems. In particular, prior work has shown that electroformed GUVs composed of a ternary mixture exhibit significant variation in areas occupied by an L_d partitioning fluorescent dye.[3] Other work has shown that individual GUVs produced from the same lipid film show significant variations in their phase behavior.[29,30] Although work has been done to compare GUV formation methods in terms of their resulting unilamellarity, capacitance, shear viscosity, and a number of defects visible by fluorescence microscopy,[31,32] compositional variability has yet to be directly examined. Quantifying this variability is critical, as lipid composition is the primary variable in all GUV-based measurements. Prior indirect measurements have found compositional standard deviations between 1 and 4 mol %.[3,33,34] Here, we directly quantify the compositional

Received: August 18, 2023
Revised: November 12, 2023
Accepted: November 22, 2023
Published: December 6, 2023

https://doi.org/10.1021/jacs.3c09039
J. Am. Chem. Soc. 2023, 145, 27521−27530

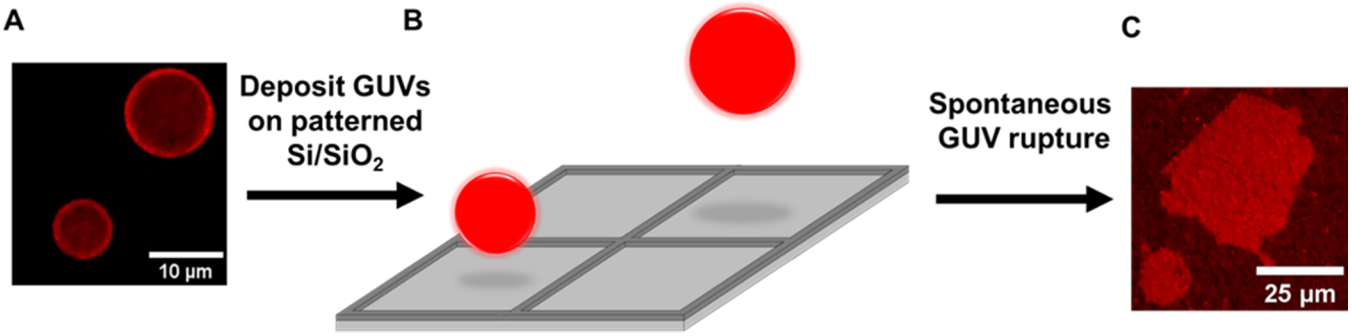

Figure 1. Experimental design. Micron-sized GUVs formed by gentle hydration or electroformation are deposited over patterned Si/SiO_2 substrates. GUVs spontaneously rupture to form individual GUV-derived planar supported bilayer patches that are subsequently freeze-dried and analyzed via NanoSIMS. (A) Epifluorescence images of POPC GUVs containing 0.1% TR-DHPE. (B) GUVs are deposited over an oxidized silicon substrate with a chrome grid and are allowed to rupture. The patterning provides a visual guide for locating patches during NanoSIMS imaging. (C) Epifluorescence images of POPC GUV patches containing 0.1% TR-DHPE. Note that if small vesicles are present within the GUV these are lost or possibly deposited elsewhere upon bilayer patch formation.

variability between individual GUVs using stable isotope labeling and secondary ion mass spectrometry (SIMS). Stable isotope labeling is not only non-perturbative (although perdeuterated lipids exhibit lower transition temperatures)[35,36] but also allows for the concentration of labeled lipids to be directly quantified.

SIMS can be used to measure isotopic ratios present in a sample with high precision.[37,38] The Cameca NanoSIMS 50L functions by collisional sputtering of a freeze-dried bilayer containing isotopically labeled lipids with primary cesium ions (Cs^+). This process ejects secondary ions, which are then separated by a mass analyzer, allowing up to seven species to be detected simultaneously. The high sensitivity and mass precision (being able to resolve species such as $^{12}C^1H^-$ and $^{13}C^-$ which have similar masses)[38,39] of the NanoSIMS 50L allows for compositional information on individual bilayers to be obtained.[38,40] For the experiments reported here, GUVs formed via either gentle hydration or electroformation were exposed to NanoSIMS substrates (10 nm SiO_2-coated Si) where they rupture to form supported bilayer patches whose area is proportional to the surface area of the parent GUV.[41,42] This process is depicted in Figure 1. In parallel, continuous supported bilayers (SLBs) were formed by conventional small vesicle fusion. SIMS can then be used to examine the compositional variability of the resulting SLBs formed by different methods. The resulting compositional variability is assessed either via external calibration curves, which determine absolute concentrations of isotopically labeled lipids in an SLB, or by examining the relative concentrations of two isotopically labeled lipids. This second method avoids relying on the accuracy of external standards and is not subject to the potential contamination of the NanoSIMS substrate. Both methods demonstrate that patches formed from individual GUVs show composition variation with standard deviations on the order of 1−4 mol % and that GUVs prepared via electroformation are less variable (standard deviations around 1−2 mol %) than GUVs formed via gentle hydration (standard deviations around 2−4 mol %). These measurements are consistent with prior indirect estimates of GUV composition.[3,33,34] Additionally, quantification of the average concentration of cholesterol in GUVs formed via gentle hydration and electroformation suggests that GUVs formed by electroformation have significantly less (around 5 mol %) cholesterol on average than GUVs formed via gentle hydration.

MATERIALS AND METHODS

All natural abundance lipids, cholesterol, and $^2H_{31}$-POPC (1-palmitoyl-2-oleoyl-*sn*-glycero-3-phosphocholine) were purchased from Avanti Polar Lipids. $^2H_7$-cholesterol was purchased from Cayman Chemical. Texas Red 1,2-dihexadecanoyl-*sn*-glycero-3-phosphoethanolamine (TR-DHPE) was purchased from Thermo Fisher Scientific. Four inch <100> p-type silicon wafers (9.5 nm SiO_2) were purchased from Silicon Quest International and were diced to 5 × 5 mm to fit in the NanoSIMS sample holder. NanoSIMS substrates were patterned with a chrome grid (5 nm height, 5 μm width) with 25, 50, or 100 μm^2 dimensions via photolithography to facilitate correlative imaging by fluorescence microscopy. All solvents were purchased from Fisher. $^{13}C_{18}$-POPC, $^{13}C_{18}$-DSPC (1,2-distearoyl-*sn*-glycero-3-phosphocholine), and ^{15}N-POPC were synthesized as previously described.[38,43] $^{13}C_{27}$-cholesterol was isolated as previously described.[44] Structures for the labeled lipids used in this study can be seen in Figure 2.

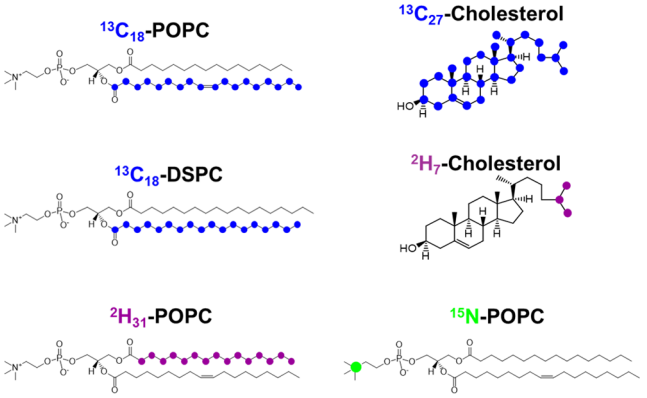

Figure 2. Isotopically labeled lipids used in this study. Color-coded circles represent the locations of isotopic labels.

Master Stock Solutions. Master stock solutions were prepared with the lipid mixture of interest dissolved in chloroform in sufficient quantities such that multiple batches of GUVs could be produced from the same vial. Master stocks were made by first adding several hundred microliters of chloroform to a 2 mL glass vial. Lipids were then added to the vial by withdrawing the appropriate volume from a pure lipid stock solution in chloroform and then injecting the volume beneath the chloroform into the master stock vial. This ensured that each lipid remained fully dissolved within the master stock. All master stocks also contained 0.1 mol % TR-DHPE so GUV patches could be examined via fluorescence microscopy once ruptured on patterned

https://doi.org/10.1021/jacs.3c09039
J. Am. Chem. Soc. 2023, 145, 27521−27530

substrates. Critically, any comparison between different methods of GUV formation was done by using lipid films produced from one of these master stocks. Also note that all lipid films were dried down at room temperature (23 ± 1 °C). Other work has suggested that films dried down at higher temperatures may yield more homogeneous GUVs[33]. This effect has not been explored further in the current work.

Gentle Hydration. Films were dried in 2 mL glass vials from Fisher. First, 200 μL of chloroform was added to a glass vial. 50 nmol of lipid in chloroform was taken from a master stock and added beneath the 200 μL of chloroform in the vial such that the lipid mixture remained dissolved. The glass vial was then vortexed, bath sonicated, and vortexed again for 30 s each. The film was then dried under a stream of argon. The vial was then placed in a desiccator overnight to remove any residual solvent. Films were then rehydrated in 0.5 mL of submicrometer-filtered 500 mM sucrose and heated to 65 ± 0.5 °C, above the melting temperature of DSPC (54.4 °C), for 15 h.

Note that while the heating temperature is above the melting point of the mixture, lower compositional variability may be attained by heating the mixture a further 10 °C above the melting point to approximately 75 °C, as has been noted by prior work.[33,45]

Electroformation. The electroformation chamber and platinum electrodes were thoroughly cleaned before the lipid films were dried on the electrodes. The chamber was first bath sonicated at 56 °C in a mixture of 7× detergent, ethanol, and deionized water in a 1:3:3 ratio. The setup was then rinsed in deionized water for 20 min before being further bath sonicated in deionized water and rinsed again with deionized water for another 20 min. The chamber was then sonicated in ethanol at room temperature. After the chamber was removed from the ethanol, the setup was dried immediately and kept in a desiccator until use. Films were formed by directly spreading 66 nmol of lipid taken from a master stock onto the platinum electrodes. After lipids were spread on the electrodes, the chamber was kept in a desiccator overnight to remove residual chloroform. The chamber was then sealed with clean glass slides and vacuum grease. Once sealed, the chamber was filled with 1.5 mL of submicrometer-filtered and degassed 500 mM sucrose before being heated to 65 ± 0.5 °C. GUVs were electroformed at 10 Hz, 3 V (peak to peak) for 2 h and then at 1 Hz, 3 V for another 30 min.

Vesicle Extrusion. Glass test tubes were filled with 200 μL of chloroform. 28 nmol of lipid from a master stock was then injected beneath chloroform in the test tube. Lipid films were then dried under argon onto the test tube sides before being desiccated overnight. Films were then resuspended in 1× phosphate-buffered saline (137 mM NaCl, 2.7 mM KCl, 8 mM $NaPO_4$, pH 7.2, submicrometer-filtered) and vortexed for 1 min. The buffer with the resuspended lipids was then passed through a membrane with 100 nm pore size 61 times while being heated to 65 °C to form SUVs (small unilamellar vesicles).

NanoSIMS Sample Preparation. GUVs were ruptured onto silicon substrates to form SLB patches after being allowed to briefly cool for 30 ± 5 min to room temperature (23 ± 1 °C). Silicon substrates were plasma cleaned for 10 min after which they were submerged in phosphate buffer (240 mM NaCl, 10 mM NaH_2PO_4 at pH 7.4). Then GUVs were deposited over the submerged substrates and allowed to incubate until approximately 10−15% of the surface was covered in SLB patches. GUV deposition was observed with a Nikon Eclipse 80i epifluorescence microscope equipped with an Andor Clara camera. The substrate and bilayers were then extensively washed with Milli-Q water. Although GUVs, particularly those formed via gentle hydration, can be multivesicular, upon GUV rupture to form an SLB patch, the internal vesicles are liberated and rinsed away. Cleaned substrates were flash frozen in liquid nitrogen and then subjected to low pressure for at least 12 h to sublimate any vitreous ice.

To form continuous bilayers on NanoSIMS substrates, 100 nm vesicles were incubated over plasma-cleaned substrates for 1 min before being washed extensively with Milli-Q water. Continuous bilayers on substrates were found to be more susceptible to dewetting during flash freezing so substrates with continuous bilayers were removed from Milli-Q water with the bilayer facing upside-down. This ensured that a drop of water remained in contact with the bilayer at all times before the substrate was flash frozen in liquid nitrogen. Once frozen, substrates were subjected to low pressure using the same method as for GUV patch samples. Lipid monolayers were formed using a KSV NIMA KN 2002 (Biolin Scientific, Stockholm, Sweden) Langmuir trough (273 cm^2) at room temperature (23 ± 1 °C). Whatman filter paper was used as a Wilhelmy plate to monitor surface pressure. Lipid mixtures dissolved in chloroform were spread on water (>18 MΩ from Milli-Q system) within the clean trough using a glass syringe. The chloroform was left to evaporate for 10 min and the barriers were compressed at 10 mm/min until the surface pressure reached 32 mN/m. Plasma-cleaned NanoSIMS substrates were glued to a glass slide and pulled through the air−water interface at a rate of 1 mm/min, while the surface pressure was maintained at 32 mN/m. Lipid monolayers were not subjected to freeze-drying, as unlike SLBs, lipid monolayers are stable in air. Both lipid monolayers and freeze-dried lipid bilayers were stored in a desiccator when not being analyzed via NanoSIMS.

NanoSIMS Analysis. Analysis was performed on a Cameca NanoSIMS 50L instrument at Stanford University. Correlative fluorescence imaging helped facilitate the selection of bilayer patches so that debris on the substrate surface were avoided. Bilayer patches were imaged with a 2pA $^{133}Cs^+$ primary beam. Ten 25 × 25 μm scans (256 × 256 pixels, 1 ms dwell time) were collected, which is enough to remove all of the deposited material on the surface. Secondary ion detectors were set to $^2H^-$, $^{12}C^-$, $^{13}C^-$, $^{12}C_2H^-$, $^{12}C_2{}^2H^-$, $^{13}C_2H^-$, and $^{13}C_2{}^2H^-$ for samples containing ^2H- or ^{13}C-labeled lipids or cholesterol. If ^{15}N-labeled POPC was contained within SLB patches, secondary ion detectors were set to $^2H^-$, $^{12}C^-$, $^{13}C^-$, $^{12}C_2H^-$, $^{12}C^{14}N^-$, $^{13}C^{15}N^-$, and $^{13}C_2{}^2H^-$. Standard samples (the calibration curves described below) were regularly analyzed to ensure that isotope ratios were reproducible from session to session.

Data Analysis. Images were analyzed using ImageJ (National Institutes of Health, USA) with the OpenMIMS plugin (National Resource for Mass Spectrometry, Harvard University USA). Planes were summed, and regions of interest were manually selected in order to exclude any debris on the sample. Total counts within each region of interest were determined via the "Tomography" tab. These counts were then used to determine the ratios of interest (typically $^2H^-/^{13}C^-$, $^{13}C^-/(^{13}C^- + ^{12}C^-)$, and $^2H^-/(^{13}C^- + ^{12}C^-)$). Calculating these ratios allows for the size of the analyzed patches to be taken into account and allows for further quantification via external calibration standards.

Calibration Standards. Concentration calibration standards were made from lipid mixtures dissolved in chloroform containing a known mol % of labeled lipid. Calibration standards used to quantify labeled lipid concentrations in ternary SLBs contained 20 mol % cholesterol, as this is present in the ternary mixture. Calibration curves without cholesterol were also prepared so that labeled lipid concentrations in mixtures without cholesterol could quantified. The prepared lipid mixtures dissolved in chloroform were spread on plasma-cleaned NanoSIMS substrates. The chloroform was then allowed to evaporate to form a lipid film. Concentration calibration standards were kept in a desiccator until use.

RESULTS AND DISCUSSION

Comparing GUV Preparation Methods via Double Labeling. First, we assessed the variability in relative concentrations of labeled lipids for different GUV preparation methods. Although direct concentration quantification via external calibration curves can give estimates of the concentration of a labeled species, this method is subject to inaccuracies. These experiments can be skewed by surface contamination and are heavily reliant on the accuracy of the calibration standards. In order to avoid these issues, and inspired by prior work,[46] initial experiments examined the relative change in ion counts from patch to patch resulting

https://doi.org/10.1021/jacs.3c09039
J. Am. Chem. Soc. 2023, 145, 27521−27530

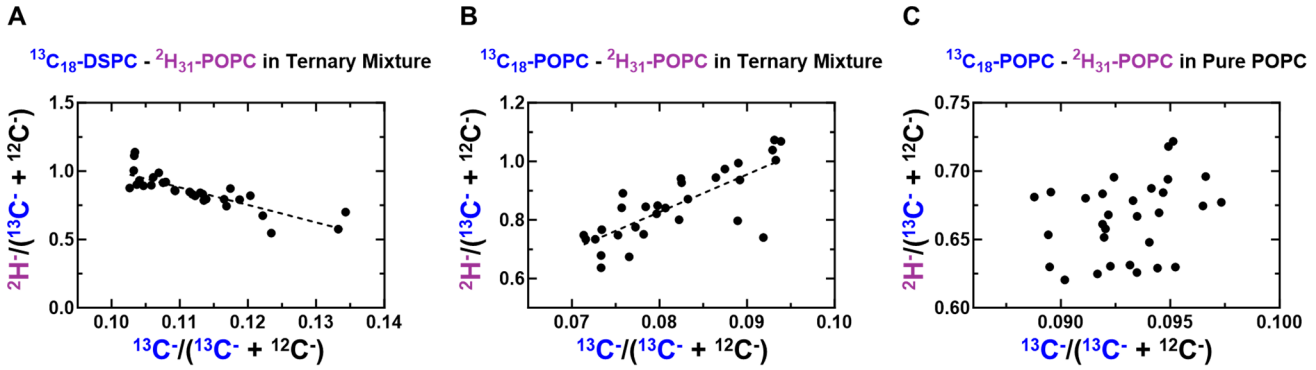

Figure 3. Concentration correlations of different labeling schemes. Correlations between the $^{2}H^{-}/(^{13}C^{-} + ^{12}C^{-})$ and $^{13}C^{-}/(^{13}C^{-} + ^{12}C^{-})$ ratios for each lipid mixture. The $^{2}H^{-}/(^{13}C^{-} + ^{12}C^{-})$ ratio tracks the amount of ^{2}H-labeled lipid in the bilayer, while the $^{13}C^{-}/(^{13}C^{-} + ^{12}C^{-})$ ratio tracks the amount of ^{13}C-labeled lipid in the bilayer. (A) Correlation between $^{2}H_{31}$-POPC and $^{13}C_{18}$-DSPC ratios in the ternary mixture DSPC:$^{13}C_{18}$-DSPC:POPC:$^{2}H_{31}$-POPC:CHOL 20:20:20:20:20. (B) Correlation between $^{2}H_{31}$-POPC and $^{13}C_{18}$-POPC ratios in the ternary mixture DSPC:$^{13}C_{18}$-POPC:$^{2}H_{31}$-POPC:CHOL 40:20:20:20. (C) Absence of correlation between $^{2}H_{31}$-POPC and $^{13}C_{18}$-POPC ratios in a pure POPC mixture with composition $^{13}C_{18}$-POPC:$^{2}H_{31}$-POPC:POPC 20:20:60.

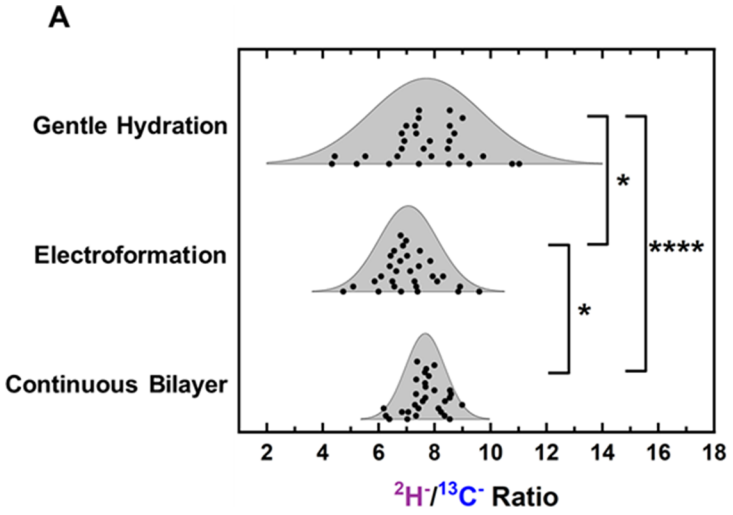

B

Method	$^{2}H^{-}/^{13}C^{-}$ Standard Deviation
Gentle Hydration	1.6
Electroformation	1.1
Continuous Bilayer	0.7

Figure 4. Measured $^{2}H^{-}/^{13}C^{-}$ ratios for different methods. GUV patches formed by gentle hydration and electroformation were compared to continuous bilayers formed from SUVs via their $^{2}H^{-}/^{13}C^{-}$ ratios. All samples were produced from a master stock with nominal composition DSPC:$^{13}C_{18}$-DSPC:POPC:$^{2}H_{31}$-POPC:CHOL 20:20:20:20:20. (A) Displays the $^{2}H^{-}/^{13}C^{-}$ ratio distributions for each preparation method. Significance was determined via an F-test. For this and subsequent plots, each point represents a measurement made on a single GUV patch or corral containing an SLB. Thirty bilayers were examined for each sample. For this and all subsequent plots, * $p \leq 0.05$, ** $p \leq 0.01$, *** $p \leq 0.001$, and **** $p \leq 0.0001$. The displayed curves are normal distributions calculated by using the standard deviation and average from the GUV patch measurements. Note that these have been overlaid to guide the reader and that the area under the curve has not been normalized. A dot plot representation of the distributions can be seen in Figure S21. (B) Calculated standard deviations of the $^{2}H^{-}/^{13}C^{-}$ ratio for each preparation method.

from two lipids with different isotopic labels. This was done with a POPC:DSPC:CHOL 40:40:20 mixture. This mixture was chosen as GUV patches with this composition do not display macroscopic phase separation between lipid components[1,4,16] within the 50 nm lateral resolution of the NanoSIMS primary ion beam (Figure S1; there is nanoscale separation present in these SLB patches which can be detected by ion recombination[43]). This mixture is also well-studied in GUVs and GUV patches.[4,43,47]

In order to determine which pair of labeled lipids is most sensitive to relative changes in concentration, two ternary samples, one with the composition $^{13}C_{18}$-DSPC:POPC:$^{2}H_{31}$-POPC:CHOL 20:20:20:20:20 and the other with the composition DSPC:$^{13}C_{18}$-POPC:$^{2}H_{31}$-POPC:CHOL 40:20:20:20 were prepared. Additionally, a sample with the composition $^{2}H_{31}$-POPC:$^{13}C_{18}$-POPC:POPC 20:20:60 was also prepared (samples with this composition are denoted as pure POPC). $^{13}C^{-}/(^{13}C^{-} + ^{12}C^{-})$ and $^{2}H^{-}/(^{13}C^{-} + ^{12}C^{-})$ ratios were then measured for 30 GUV patches formed via gentle hydration for all three samples.

Figure 3 shows the correlation between the $^{2}H^{-}/(^{13}C^{-} + ^{12}C^{-})$ and $^{13}C^{-}/(^{13}C^{-} + ^{12}C^{-})$ ratios for each labeling scheme. The $^{2}H^{-}/(^{13}C^{-}+^{12}C^{-})$ ratio tracks the amount of ^{2}H-labeled lipid in the bilayer, while the $^{13}C^{-}/(^{13}C^{-} + ^{12}C^{-})$ ratio tracks the amount of ^{13}C-labeled lipid in the bilayer. Figure 3 demonstrates that the correlation between the ratios is a function of both the location of the isotopic label and the overall composition of the bilayer. The ternary mixture containing both $^{2}H_{31}$-POPC and $^{13}C_{18}$-POPC displays a positive correlation between the lipid concentrations. Conversely, the ternary mixture containing $^{2}H_{31}$-POPC and $^{13}C_{18}$-DSPC displays a clear negative correlation between the

https://doi.org/10.1021/jacs.3c09039
J. Am. Chem. Soc. 2023, 145, 27521−27530

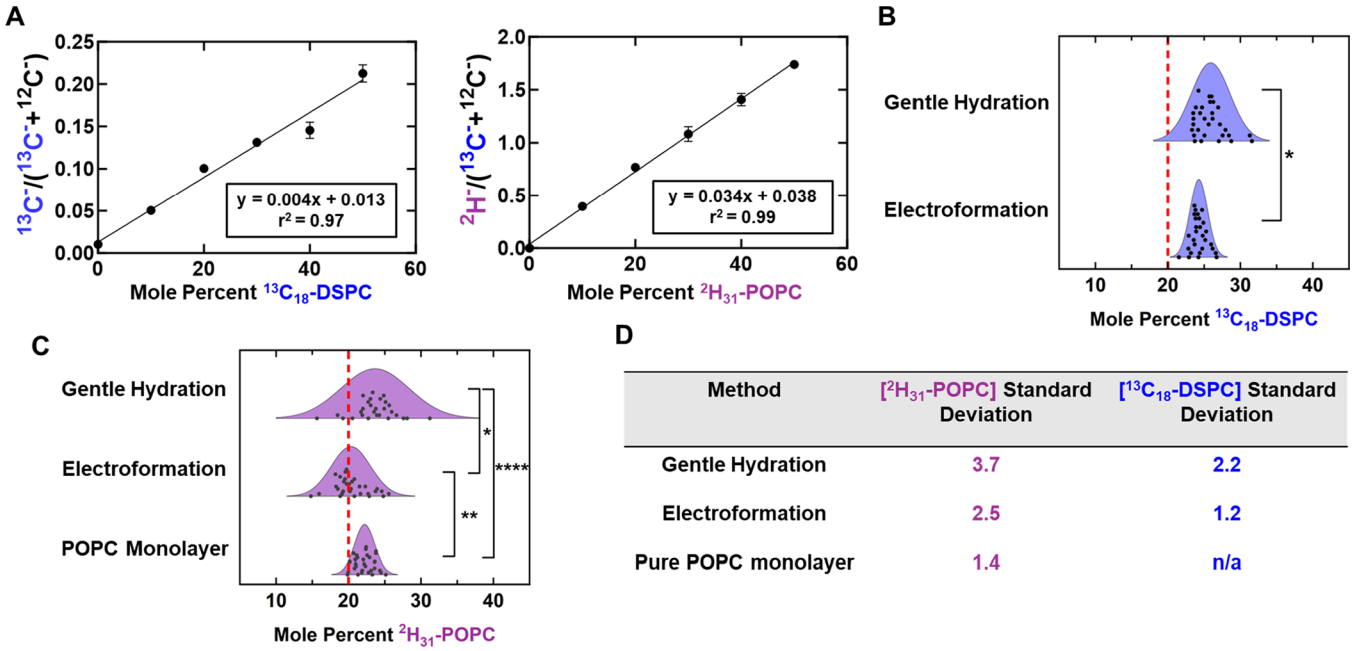

Method	[$^2H_{31}$-POPC] Standard Deviation	[$^{13}C_{18}$-DSPC] Standard Deviation
Gentle Hydration	3.7	2.2
Electroformation	2.5	1.2
Pure POPC monolayer	1.4	n/a

Figure 5. Concentration quantification of GUV patches and monolayers. (A) Representative calibration curves for $^{13}C_{18}$-DSPC and $^2H_{31}$-POPC. (B) Calculated $^{13}C_{18}$-DSPC concentration distributions for GUV patches formed by gentle hydration and electroformation. All GUVs were formed using a ternary mixture with nominal composition DSPC:$^{13}C_{18}$-DSPC:POPC:$^2H_{31}$-POPC:CHOL 20:20:20:20:20. The gentle hydration $^{13}C_{18}$-DSPC concentration distribution is significantly different relative to the corresponding electroformation distribution, as determined by F-test. Red dashed lines indicate the nominal concentration of labeled lipids. (C) Displays the calculated $^2H_{31}$-POPC concentration distributions for GUV patches formed by gentle hydration and electroformation. These concentration distributions are compared to $^2H_{31}$-POPC concentrations measured in a monolayer composed of POPC with 20 mol % of $^2H_{31}$-POPC. Dot plot representations of these distributions can be seen in Figure S22. (D) Calculated standard deviations for each concentration distribution.

concentrations of the two components. These trends can be attributed to preferential interactions between $^{13}C_{18}$-POPC and $^2H_{31}$-POPC and unfavorable interactions between $^{13}C_{18}$-DSPC and $^2H_{31}$-POPC within ternary bilayers.

As shown in Figure 3C, pure POPC SLBs containing $^2H_{31}$-POPC and $^{13}C_{18}$-POPC did not show any clear correlation in concentration between the differently labeled lipids. $^2H_{31}$-POPC, $^{13}C_{18}$-POPC, and natural abundance POPC within the pure POPC mixture only differ from each other in terms of isotopic labeling. As a result, when the concentration of one labeled component is higher in a GUV, the extent to which it replaces either the other labeled or unlabeled component is essentially random.

Based on the results from Figure 3, a ternary mixture containing $^{13}C_{18}$-DSPC and $^2H_{31}$-POPC is expected to be the most sensitive to relative concentration changes between the two labeled lipids, as the concentrations of these two components are anticorrelated. Therefore, this mixture was used to study the compositional variability of GUVs formed by electroformation or gentle hydration.

GUVs with this composition were generated from the same master stock by either gentle hydration or electroformation. The same master stock was also used to generate 100 nm SUVs which were then ruptured onto NanoSIMS substrates to form continuous bilayers within the corrals of the patterned NanoSIMS substrate. Since these continuous bilayers are formed from hundreds of SUVs, the relative concentrations of $^{13}C_{18}$-DSPC and $^2H_{31}$-POPC should be more consistent than in SLB patches formed from the rupture of a single GUV. The measured $^2H^-/^{13}C^-$ ratio for 30 individual bilayer patches or 30 corrals containing continuous bilayers is shown in Figure 4. Based on the measured ratios, gentle hydration has the highest standard deviation, ±1.6, in relative concentration. The standard deviation for GUVs formed via electroformation is significantly (determined via *F*-test) lower at ±1.1. The normality of each distribution assessed by F-test as is further discussed in Section 2 of the Supporting Information. Continuous bilayers formed from SUVs have the lowest standard deviation in relative concentration, at ±0.7. Replicate samples produced from films dried from the same master stock also suggest that electroformation is less compositionally variable (lower measured standard deviations) than gentle hydration (Figure S4).

The raw data for all of the distributions in the main text and the Supporting Information can be seen in Section 16 of the Supporting Information. Additionally, each distribution presented is replotted as a dot plot in Section 17 of the Supporting Information to provide a second way to visualize the data.

Absolute Concentration Variability. Although measuring the $^2H^-/^{13}C^-$ ratio is useful for comparing the variability in different methods while avoiding concerns regarding surface contamination and calibration accuracy (further discussed in Section 4 of the Supporting Information), quantification of absolute concentration is useful for determining how much the mol % of a particular lipid varies from GUV to GUV. Therefore, external calibration curves, such as those shown in Figure 5A, were used to relate quantitative ion ratios to labeled lipid concentrations. This allowed the concentration of each labeled species within one GUV patch to be determined. This analysis was performed for the GUV samples discussed in Figure 4.

As shown in Figure 5B,C, GUV patches produced via electroformation showed consistently lower standard deviations in both $^{13}C_{18}$-DSPC and $^2H_{31}$-POPC concentrations than

https://doi.org/10.1021/jacs.3c09039
J. Am. Chem. Soc. 2023, 145, 27521−27530

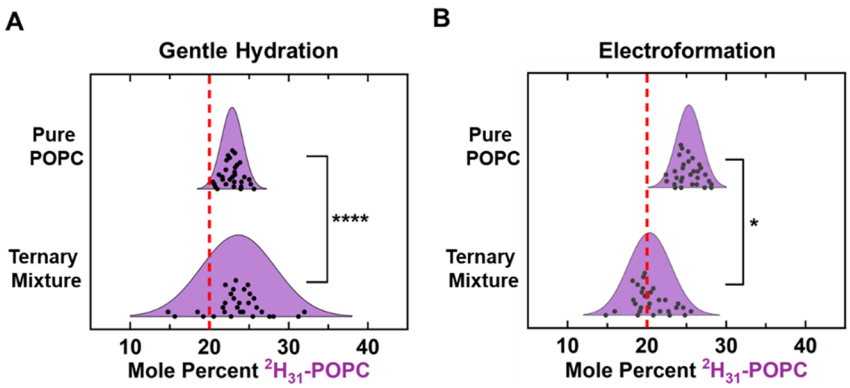

C

Method	[$^{2}H_{31}$-POPC] Standard Deviation	
	Pure POPC	Ternary Mixture
Gentle Hydration	1.4	3.7
Electroformation	1.6	2.5

Figure 6. Pure and ternary mixture concentration variability. $^{2}H_{31}$-POPC concentrations of individual GUV patches composed with pure POPC ($^{13}C_{18}$-POPC:$^{2}H_{31}$-POPC:POPC 20:20:60) or ternary ($^{13}C_{18}$-DSPC:POPC:$^{2}H_{31}$-POPC:CHOL 20:20:20:20:20) compositions were compared. Both pure POPC and ternary GUVs were formed by either electroformation (A) or gentle hydration (B). For both methods, the patches composed of pure POPC display significantly less $^{2}H_{31}$-POPC concentration variability than that of ternary patches formed using the same method. Dot plot representations of these distributions can be seen in Figure S23. (C) Displays the calculated standard deviations for each sample.

those formed via gentle hydration as demonstrated by the calculated standard deviations and supported by a corresponding F-test. To determine the lower bound on variability (i.e., how much of the variation in concentration measurements is due to instrument noise and surface contamination), a monolayer with overall composition $^{2}H_{31}$-POPC:$^{13}C_{18}$-POPC:-POPC 20:20:60 (pure POPC composition) was formed on a NanoSIMS substrate and compared to both GUV samples. Since a monolayer should be compositionally homogeneous across the substrate surface, this measurement can be used to approximate how much of the variability (the measured standard deviation) is due to the experimental method. As seen in Figure 5C, measurements on pure POPC monolayers resulted in a lower standard deviation in $^{2}H_{31}$-POPC concentrations than that measured in GUVs formed via electroformation or gentle hydration (±1.4 mol % for monolayers, ±2.5 mol % for electroformed GUVs, and ±3.7 mol % for GUVs formed by gentle hydration). However, these monolayers cannot be compared via the $^{2}H^{-}/^{13}C^{-}$ ratio as was done in Figure 4 because the correlation between $^{2}H_{31}$-POPC and $^{13}C_{18}$-POPC concentrations in pure POPC is dramatically different from the correlation between $^{2}H_{31}$-POPC and $^{13}C_{18}$-DSPC in ternary mixtures (Figure 3). Additionally, ternary monolayers formed from the ternary master stock containing $^{2}H_{31}$-POPC and $^{13}C_{18}$-DSPC display macroscale separation (Figure S6) and are therefore not comparable to the GUV samples, as is further discussed in Section 5 of the Supporting Information. Therefore, monolayers can be compared to GUV samples only via absolute concentrations. Additional analysis suggests that the size of the region selected for quantification within the 25 × 25 μm analysis region does not significantly impact the distributions shown in Figures 4 and 5 (further discussed in Section 6 of the Supporting Information). Therefore, the intrinsic signal-to-noise ratio of a single patch is unlikely to substantially impact the GUV variability observed for different formation methods. It should be noted that the absolute values measured for isotope-labeled lipid concentrations demonstrate deviation from the nominal concentrations in the master stock solution. In some cases, the labeled lipid concentration deviates by 5−6 mol % from the expected concentration. This is likely the result of multiple factors including substrate surface contamination by ^{12}C, the accuracy of the external calibration curves, and error involved in preparing labeled lipid stock solutions (which are then used to make master stocks).

Sources of Variability. In order to further explore sources of the observed GUV variability, GUVs with pure POPC composition ($^{2}H_{31}$-POPC:$^{13}C_{18}$-POPC:POPC 20:20:60) were formed by either gentle hydration or electroformation. Thirty GUV patches with this composition were analyzed for each method, and their absolute concentrations were determined via external calibration curves. In Figure 6, the calculated $^{2}H_{31}$-POPC concentrations in pure POPC samples are compared to the $^{2}H_{31}$-POPC concentrations in the previously discussed ternary mixture. Ternary GUV patches formed either by electroformation or gentle hydration have higher measured standard deviations in $^{2}H_{31}$-POPC concentrations relative to pure POPC patches formed by the same method (Figure 6C). This lower variability for the pure POPC GUVs can also be seen for the $^{13}C_{18}$-labeled lipids (Figure S9). These results suggest that more complex lipid compositions lead to considerably more compositional variability. It also suggests that the observed compositional variability is not solely due to residual contamination of either the platinum electrodes used for electroformation or the glass vials used for gentle hydration. If these surfaces had significant contamination, pure POPC patches would have compositional variability comparable to that of ternary patches. Comparison of $^{2}H_{31}$-POPC concentration variability between pure POPC patches formed via either electroformation or gentle hydration did not show a significant difference in compositional variability (Figure S10). This suggests that the higher standard deviations observed in GUV patches formed via gentle hydration (Figures 4 and 5) are not due to higher residual contamination on glass vials relative to the platinum electrodes but rather result from the complexity of the ternary mixture and the method of GUV formation. Additionally, the average $^{2}H^{-}$, $^{12}C^{-}$, and $^{13}C^{-}$ counts were compared between regions of interest with and without a bilayer to gauge the level of contamination on the substrate surface (Figure S11). Regions of interest containing bilayer showed considerably higher signal on all detectors than regions of interest in an exposed substrate. Further analysis was also performed to correct the observed variabilities in ternary GUV patches for noise due to sample preparation and analysis (discussed in Section 10 of the Supporting Information).

https://doi.org/10.1021/jacs.3c09039
J. Am. Chem. Soc. 2023, 145, 27521−27530

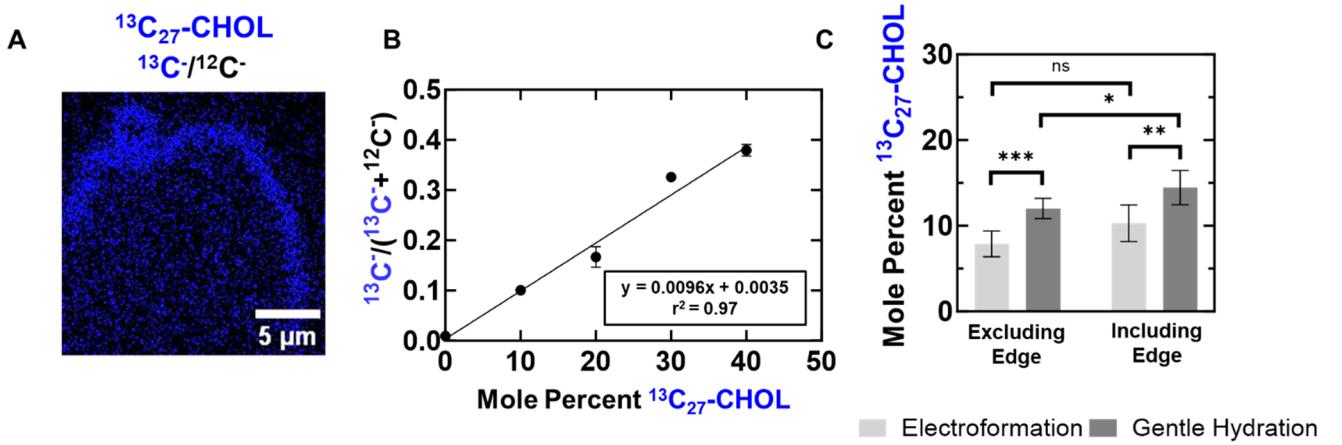

Figure 7. Cholesterol concentration differences between electroformation and gentle hydration. GUVs were formed via electroformation or gentle hydration from a master stock with nominal composition DSPC:POPC:$^{2}H_{31}$-POPC:$^{13}C_{27}$-CHOL 40:20:20:20. (A) NanoSIMS image of a GUV patch formed via electroformation, which shows significant localization of $^{13}C_{27}$-CHOL to the edge of the GUV patch. (B) $^{13}C_{27}$-CHOL calibration curve. (C) Comparison of $^{13}C_{27}$-CHOL concentration in GUV patches formed via gentle hydration or electroformation. Error bars represent 95% confidence intervals. Comparisons were conducted either excluding the edge of the bilayer patch or including the edge of the bilayer patch. Regardless of the analysis method, electroformed GUVs contained less cholesterol on average. Replicate sample quantification along with internal controls ($^{2}H_{31}$-POPC concentration quantification) can be found in Figures S19 and S20 of the Supporting Information.

To further examine potential sources of variability, lipid films from the master stock containing $^{13}C_{18}$-DSPC and $^{2}H_{31}$-POPC were dried directly on NanoSIMS substrates and imaged. No significant separation within the 50 nm lateral resolution of the NanoSIMS was observed between $^{13}C_{18}$-DSPC and $^{2}H_{31}$-POPC within the film (Figure S13). However, atomic recombination experiments demonstrated that there is nanoscale separation between POPC and DSPC within the film (Figure S14). These preferential interactions within the film may contribute to lipid sorting while GUVs are being formed.

Additional experiments also suggest that the size of the GUV patch analyzed is not correlated with either $^{13}C_{18}$-DSPC or $^{2}H_{31}$-POPC concentrations (Section 12 of the Supporting Information). Furthermore, additional data suggest that two different GUVs typically do not rupture to form one patch (Section 13 of the Supporting Information). This suggests that most patches are the product of a single GUV and that minimal compositional averaging between GUVs occurs.

The measured standard deviations as well as the corrected standard deviations (Section 10 of the Supporting Information) agree relatively well with indirect measurements of GUV-to-GUV compositional variation. Prior work using fluorescence microscopy to quantify the area fraction occupied by optically resolvable domains approximated a ±2.1 mol % standard deviation in electroformed DOPC/eSM/CHOL GUVs. Similarly, estimates from GUV transition temperatures measure a standard deviation of approximately ±2[45] or ±4 mol % for electroformed GUVs. These results are in relatively good agreement with the direct measurements presented here, where we measure standard deviations around 1−2 mol % for electroformed GUVs and 2−4 mol % for GUVs formed via gentle hydration. However, it should be noted that we used DSPC for this study, which is a higher melting point lipid and may lend itself to slightly greater variability due to the high temperatures (T_m = 54.4 °C) needed to keep this lipid fluid.

Quantifying Cholesterol Concentrations. Cholesterol concentration was also examined in the GUV patches. Unlike phospholipids, Cholesterol localized significantly to the edges of GUV patches formed by either electroformation or gentle hydration as seen in Figures 7A and S18. This observation is consistent with work from other groups, who have noted that L_o domains can localize to the edge of GUV patches[42,48] although other work has suggested that L_d domains can also partition to patch edges,[49] suggesting that this effect may depend on the composition examined. However, for the composition examined here, we observe cholesterol (presumably in L_o domains) partitioning to the edges of bilayer patches. This partitioning makes quantification of cholesterol variability in GUVs significantly more challenging as the relative ratio of edge to center within the analyzed region needs to be considered as well as how the overall concentration of cholesterol in a patch may affect its partitioning between the edge and center. As a result, the variability in cholesterol concentration from GUV to GUV was not assessed. Instead, the average cholesterol concentration was determined for different GUV formation methods. Ternary GUV patches were formed via gentle hydration and electroformation using a master stock with nominal composition DSPC:POPC:$^{2}H_{31}$-POPC:$^{13}C_{27}$-CHOL 40:20:20:20. The average concentration was then calculated by either including or excluding the cholesterol-rich edges. Regardless of the analysis method used, the average concentration of cholesterol was lower in electroformed GUV patches, as can be seen in Figure 7C. The average $^{2}H_{31}$-POPC concentration was the same between the two methods regardless of the analysis method (Figure S19). Average cholesterol concentration was also examined in GUV patches where all three components are isotopically labeled (Figure S18). These experiments also demonstrate lower average cholesterol concentrations in the electroformed GUVs.

Although there appears to be cholesterol partitioning to the edge of bilayer patches, the increase in cholesterol concentration when the edge is included in the analysis relative to when it is excluded appears to be moderate. There is only a statistically significant difference between the analysis methods (p = 0.03), for GUVs formed via gentle hydration (Figure 7C). Replicate samples (Figure S20) do not reproduce this

https://doi.org/10.1021/jacs.3c09039
J. Am. Chem. Soc. 2023, 145, 27521−27530

difference between the analysis methods. These replicates are of critical importance, as they suggest that the changes in cholesterol concentration are likely not an artifact resulting from the challenges associated with measuring absolute concentrations, as discussed at the end of the previous section.

The source of the difference in cholesterol concentrations between GUVs formed by electroformation and those formed by gentle hydration may be the result of the alternating current applied during electroformation. While the phospholipids present in the ternary mixture are zwitterionic and potentially more affected by the alternating current applied during electroformation, cholesterol is neutral and therefore may be less responsive to the applied current. This would result in a lower incorporation into electroformed GUVs. However, the experiments performed here cannot provide a definitive explanation or mechanism for the difference in cholesterol concentrations between the two methods. Additionally, it should be noted that prior measurements suggest that hydrated films[50,51] have comparable cholesterol solubility limits to electroformed films.[52] These results imply that both methods lead to equivalent cholesterol concentrations and disagree with the results presented here.

CONCLUSIONS

GUVs are a widely used model system for probing lipid−protein and lipid−lipid[53,54] interactions. Despite the widespread use of GUVs, little work has been done to probe GUV-to-GUV compositional variation. This is likely due to the lack of methods to accurately assess the concentration of a given lipid within a single GUV. The Cameca NanoSIMS 50L allows for high-precision determination of the concentration of individual lipid species via non-perturbative stable isotope labeling.

Here, we demonstrate that variability on the order of 1−4 mol % is present in GUVs composed of a ternary DSPC:POPC:CHOL mixture. It is shown that GUVs formed via electroformation have considerably less compositional variability than those formed via gentle hydration (GUVs formed by electroformation have concentration standard deviations of 1−2 mol % compared to the 2−4 mol % of GUVs formed via gentle hydration). This is true regardless of whether the relative change in concentration between two labeled species is calculated or if the variability in the absolute concentration is determined via external calibration curves. Although the mechanism behind the lower variability seen in electroformed GUVs is unclear, it is clear that ternary mixtures are far more variable than pure mixtures and that preferential interactions between certain lipids are present in the films used to form ternary GUVs.

Although the variability in cholesterol concentration is not examined here, the average concentration of labeled cholesterol was compared between different methods. This demonstrated that electroformed GUVs have a lower average cholesterol concentration. Additionally, it is worth noting that other potential disadvantages have been reported with electroformation that are not discussed here.[55] Therefore, while electroformation may yield more compositionally uniform GUVs, there are downsides to the method that must be considered.

ASSOCIATED CONTENT

Supporting Information

The Supporting Information is available free of charge at https://pubs.acs.org/doi/10.1021/jacs.3c09039.

Choice of lipid mixture; normality verification for F-tests; replicate electroformation and gentle hydration samples; verification of absolute calibration accuracy; ternary monolayers; effect of analysis area on concentration distributions; ^{13}C-labeled lipid comparisons in pure and ternary mixtures; comparison of pure POPC mixtures with different methods; detector counts on bilayer and exposed substrates; correcting ternary GUV compositional variability; nanoscale heterogeneity in lipid films; relation between GUV patch size and $^{13}C_{18}$-DSPC and $^{2}H_{31}$-POPC concentrations; assessing the extent of GUV mixing during patch formation; tracking cholesterol concentration in triply labeled bilayers; assessing average $^{2}H_{31}$-POPC concentration in $^{13}C_{27}$-CHOL containing patches; tabulated raw GUV composition data; dot plot representations of GUV composition distributions (PDF)

AUTHOR INFORMATION

Corresponding Author

Steven G. Boxer − *Department of Chemistry, Stanford University, Stanford, California 94305-5012, United States;* orcid.org/0000-0001-9167-4286; Email: sboxer@stanford.edu

Authors

Dashiel S. Grusky − *Department of Chemistry, Stanford University, Stanford, California 94305-5012, United States;* orcid.org/0000-0002-0145-398X

Ahanjit Bhattacharya − *Department of Chemistry, Stanford University, Stanford, California 94305-5012, United States*

Complete contact information is available at: https://pubs.acs.org/10.1021/jacs.3c09039

Notes

The authors declare no competing financial interest.

ACKNOWLEDGMENTS

This work was supported by grants from the NSF (MCB-1915727) and NIH (R35GM118044) to S.G.B. The Cameca NanoSIMS 50L at the Stanford Nano Shared Facilities (SNSF) was supported by the National Science Foundation (ECCS-2026822). We thank Christie Jilly-Rehak and Matthew Mills at the Stanford Nanocharacterization Laboratory for instrument support on the NanoSIMS 50L.

REFERENCES

(1) Heberle, F. A.; Wu, J.; Goh, S. L.; Petruzielo, R. S.; Feigenson, G. W. Comparison of Three Ternary Lipid Bilayer Mixtures: FRET and ESR Reveal Nanodomains. *Biophys. J.* **2010**, *99* (10), 3309−3318.

(2) Veatch, S. L.; Keller, S. L. Miscibility Phase Diagrams of Giant Vesicles Containing Sphingomyelin. *Phys. Rev. Lett.* **2005**, *94* (14), No. 148101.

(3) Bezlyepkina, N.; Gracià, R. S.; Shchelokovskyy, P.; Lipowsky, R.; Dimova, R. Phase Diagram and Tie-Line Determination for the Ternary Mixture DOPC/eSM/Cholesterol. *Biophys. J.* **2013**, *104* (7), 1456−1464.

(4) Konyakhina, T. M.; Wu, J.; Mastroianni, J. D.; Heberle, F. A.; Feigenson, G. W. Phase Diagram of a 4-Component Lipid Mixture:

DSPC/DOPC/POPC/Chol. *Biochim. Biophys. Acta BBA - Biomembr.* **2013**, *1828* (9), 2204−2214.
(5) Jørgensen, I. L.; Kemmer, G. C.; Pomorski, T. G. Membrane Protein Reconstitution into Giant Unilamellar Vesicles: A Review on Current Techniques. *Eur. Biophys. J.* **2017**, *46* (2), 103−119.
(6) Shi, Z.; Sachs, J. N.; Rhoades, E.; Baumgart, T. Biophysics of α-Synuclein Induced Membrane Remodelling. *Phys. Chem. Chem. Phys.* **2015**, *17* (24), 15561−15568.
(7) Doeven, M. K.; Folgering, J. H. A.; Krasnikov, V.; Geertsma, E. R.; Van den bogaart, G.; Poolman, B. Distribution, Lateral Mobility and Function of Membrane Proteins Incorporated into Giant Unilamellar Vesicles. *Biophys. J.* **2005**, *88* (2), 1134−1142.
(8) Islam, Md. Z.; Ariyama, H.; Alam, J. Md.; Yamazaki, M. Entry of Cell-Penetrating Peptide Transportan 10 into a Single Vesicle by Translocating Across Lipid Membrane and Its Induced Pores. *Biochemistry* **2014**, *53* (2), 386−396.
(9) Aimon, S.; Callan-jones, A.; Berthaud, A.; Pinot, M.; Toombes, G. E. S.; Bassereau, P. Membrane Shape Modulates Transmembrane Protein Distribution. *Dev. Cell* **2014**, *28* (2), 212−218.
(10) Garten, M.; Aimon, S.; Bassereau, P.; Toombes, G. E. S. Reconstitution of a Transmembrane Protein, the Voltage-Gated Ion Channel, KvAP, into Giant Unilamellar Vesicles for Microscopy and Patch Clamp Studies. *J. Vis. Exp.* **2015**, No. 95, No. e52281.
(11) Göpfrich, K.; Haller, B.; Staufer, O.; Dreher, Y.; Mersdorf, U.; Platzman, I.; Spatz, J. P. One-Pot Assembly of Complex Giant Unilamellar Vesicle-Based Synthetic Cells. *ACS Synth. Biol.* **2019**, *8* (5), 937−947.
(12) Noireaux, V.; Libchaber, A. A Vesicle Bioreactor as a Step toward an Artificial Cell Assembly. *Proc. Natl. Acad. Sci. U. S. A.* **2004**, *101* (51), 17669−17674.
(13) Nomura, S. M.; Tsumoto, K.; Hamada, T.; Akiyoshi, K.; Nakatani, Y.; Yoshikawa, K. Gene Expression within Cell-Sized Lipid Vesicles. *ChemBioChem* **2003**, *4*, 1172−1175.
(14) Kurihara, K.; Tamura, M.; Shohda, K.; Toyota, T.; Suzuki, K.; Sugawara, T. Self-Reproduction of Supramolecular Giant Vesicles Combined with the Amplification of Encapsulated DNA. *Nat. Chem.* **2011**, *3* (10), 775−781.
(15) Bagatolli, L. A.; Gratton, E. Two Photon Fluorescence Microscopy of Coexisting Lipid Domains in Giant Unilamellar Vesicles of Binary Phospholipid Mixtures. *Biophys. J.* **2000**, *78* (1), 290−305.
(16) Zhao, J.; Wu, J.; Heberle, F. A.; Mills, T. T.; Klawitter, P.; Huang, G.; Costanza, G.; Feigenson, G. W. Phase Studies of Model Biomembranes: Complex Behavior of DSPC/DOPC/Cholesterol. *Biochim. Biophys. Acta BBA - Biomembr.* **2007**, *1768* (11), 2764−2776.
(17) Zhao, J.; Wu, J.; Shao, H.; Kong, F.; Jain, N.; Hunt, G.; Feigenson, G. Phase Studies of Model Biomembranes: Macroscopic Coexistence of Lα+Lβ, with Light-Induced Coexistence of Lα+Lo Phases. *Biochim. Biophys. Acta BBA - Biomembr.* **2007**, *1768* (11), 2777−2786.
(18) Konyakhina, T. M.; Goh, S. L.; Amazon, J.; Heberle, F. A.; Wu, J.; Feigenson, G. W. Control of a Nanoscopic-to-Macroscopic Transition: Modulated Phases in Four-Component DSPC/DOPC/POPC/Chol Giant Unilamellar Vesicles. *Biophys. J.* **2011**, *101* (2), L8−L10.
(19) Wang, H.-Y.; Chan, S. H.; Dey, S.; Castello-serrano, I.; Rosen, M. K.; Ditlev, J. A.; Levental, K. R.; Levental, I. Coupling of Protein Condensates to Ordered Lipid Domains Determines Functional Membrane Organization. *Sci. Adv.* **2023**, *9*, No. eadf6205, DOI: 10.1126/sciadv.adf6205.
(20) Veatch, S. L.; Polozov, I. V.; Gawrisch, K.; Keller, S. L. Liquid Domains in Vesicles Investigated by NMR and Fluorescence Microscopy. *Biophys. J.* **2004**, *86* (5), 2910−2922.
(21) Angelova, M. I.; Soléau, S.; Méléard, Ph.; Faucon, F.; Bothorel, P. Preparation of Giant Vesicles by External AC Electric Fields Kinetics and Applications. *Prog. Colloid Polym. Sci.* **1992**, *89*, 127−131.
(22) Herold, C.; Chwastek, G.; Schwille, P.; Petrov, E. P. Efficient Electroformation of Supergiant Unilamellar Vesicles Containing Cationic Lipids on ITO-Coated Electrodes. *Langmuir* **2012**, *28* (13), 5518−5521.
(23) Reeves, J. P.; Dowben, R. M. Formation and Properties of Thin-Walled Phospholipid Vesicles. *J. Cell. Physiol.* **1969**, *73* (1), 49−60.
(24) Darszon, A.; Vandenberg, C. A.; Schönfeld, M.; Ellisman, M. H.; Spitzer, N. C.; Montal, M. Reassembly of Protein-Lipid Complexes into Large Bilayer Vesicles: Perspectives for Membrane Reconstitution. *Proc. Natl. Acad. Sci. U. S. A.* **1980**, *77* (1), 239−243.
(25) Needham, D.; Mcintosh, T. J.; Evans, E. Thermomechanical and Transition Properties of Dimyristoylphosphatidylcholine/Cholesterol Bilayers. *Biochemistry* **1988**, *27* (13), 4668−4673.
(26) Angelova, M. I.; Dimitrov, D. S. Liposome Electroformation. *Faraday Discuss. Chem. Soc.* **1986**, *81*, 303−311.
(27) Dimitrov, D. S.; Angelova, M. I. Lipid Swelling and Liposome Formation Mediated by Electric Fields. *Biochem. Bioenerg.* **1988**, *19* (2), 323−336.
(28) Dimitrov, D. S. ; Angelova, M. I. Lipid Swelling and Liposome Formation on Solid Surfaces in External Electric Fields. In *New Trends in Colloid Science*; Hoffmann, H., Ed.; Progress in Colloid & Polymer Science: Steinkopff: Darmstadt, 1987; Vol. *73*, pp. 48−56.
(29) Groves, J. T. Bending Mechanics and Molecular Organization in Biological Membranes. *Annu. Rev. Phys. Chem.* **2007**, *58* (1), 697−717.
(30) Rozovsky, S.; Kaizuka, Y.; Groves, J. T. Formation and Spatio-Temporal Evolution of Periodic Structures in Lipid Bilayers. *J. Am. Chem. Soc.* **2005**, *127* (1), 36−37.
(31) Rodriguez, N.; Pincet, F.; Cribier, S. Giant Vesicles Formed by Gentle Hydration and Electroformation: A Comparison by Fluorescence Microscopy. *Colloids Surf. B Biointerfaces* **2005**, *42* (2), 125−130.
(32) Faizi, H. A.; Tsui, A.; Dimova, R.; Vlahovska, P. M. Bending Rigidity, Capacitance, and Shear Viscosity of Giant Vesicle Membranes Prepared by Spontaneous Swelling, Electroformation, Gel-Assisted, and Phase Transfer Methods: A Comparative Study. *Langmuir* **2022**, *38* (34), 10548−10557.
(33) Veatch, S. L.; Keller, S. L. Seeing Spots: Complex Phase Behavior in Simple Membranes. *Biochim. Biophys. Acta BBA - Mol. Cell Res.* **2005**, *1746* (3), 172−185.
(34) Baykal-caglar, E.; Hassan-zadeh, E.; Saremi, B.; Huang, J. Preparation of Giant Unilamellar Vesicles from Damp Lipid Film for Better Lipid Compositional Uniformity. *Biochim. Biophys. Acta BBA - Biomembr.* **2012**, *1818* (11), 2598−2604.
(35) Bryant, G.; Taylor, M. B.; Darwish, T. A.; Krause-heuer, A. M.; Kent, B.; Garvey, C. J. Effect of Deuteration on the Phase Behaviour and Structure of Lamellar Phases of Phosphatidylcholines − Deuterated Lipids as Proxies for the Physical Properties of Native Bilayers. *Colloids Surf. B Biointerfaces* **2019**, *177*, 196−203.
(36) Veatch, S. L.; Gawrisch, K.; Keller, S. L. Closed-Loop Miscibility Gap and Quantitative Tie-Lines in Ternary Membranes Containing Diphytanoyl PC. *Biophys. J.* **2006**, *90* (12), 4428−4436.
(37) Hauri, E. H.; Papineau, D.; Wang, J.; Hillion, F. High-Precision Analysis of Multiple Sulfur Isotopes Using NanoSIMS. *Chem. Geol.* **2016**, *420*, 148−161.
(38) Kraft, M. L.; Weber, P. K.; Longo, M. L.; Hutcheon, I. D.; Boxer, S. G. Phase Separation of Lipid Membranes Analyzed with High-Resolution Secondary Ion Mass Spectrometry. *Science* **2006**, *313* (5795), 1948−1951.
(39) Lozano, M. M.; Liu, Z.; Sunnick, E.; Janshoff, A.; Kumar, K.; Boxer, S. G. Colocalization of the Ganglioside G_{M1} and Cholesterol Detected by Secondary Ion Mass Spectrometry. *J. Am. Chem. Soc.* **2013**, *135* (15), 5620−5630.
(40) Boxer, S. G.; Kraft, M. L.; Weber, P. K. Advances in Imaging Secondary Ion Mass Spectrometry for Biological Samples. *Annu. Rev. Biophys.* **2009**, *38* (1), 53−74.
(41) Ngassam, V. N.; Su, W.-C.; Gettel, D. L.; Deng, Y.; Yang, Z.; Wang-tomic, N.; Sharma, V. P.; Purushothaman, S.; Parikh, A. N. Recurrent Dynamics of Rupture Transitions of Giant Lipid Vesicles at Solid Surfaces. *Biophys. J.* **2021**, *120* (4), 586−597.

(42) Bleecker, J. V.; Cox, P. A.; Foster, R. N.; Litz, J. P.; Blosser, M. C.; Castner, D. G.; Keller, S. L. Thickness Mismatch of Coexisting Liquid Phases in Noncanonical Lipid Bilayers. *J. Phys. Chem. B* **2016**, *120* (10), 2761−2770.
(43) Grusky, D. S.; Moss, F. R.; Boxer, S. G. Recombination between ^{13}C and ^{2}H to Form Acetylide ($^{13}C_2{}^{2}H^-$) Probes Nanoscale Interactions in Lipid Bilayers via Dynamic Secondary Ion Mass Spectrometry: Cholesterol and GM_1 Clustering. *Anal. Chem.* **2022**, *94* (27), 9750−9757.
(44) Lozano, M. M.; Hovis, J. S.; Moss, F. R.; Boxer, S. G. Dynamic Reorganization and Correlation among Lipid Raft Components. *J. Am. Chem. Soc.* **2016**, *138* (31), 9996−10001.
(45) Veatch, S. L.; Keller, S. L. Separation of Liquid Phases in Giant Vesicles of Ternary Mixtures of Phospholipids and Cholesterol. *Biophys. J.* **2003**, *85* (5), 3074−3083.
(46) Larsen, J.; Hatzakis, N. S.; Stamou, D. Observation of Inhomogeneity in the Lipid Composition of Individual Nanoscale Liposomes. *J. Am. Chem. Soc.* **2011**, *133* (28), 10685−10687.
(47) Moss, F. R.; Boxer, S. G. Atomic Recombination in Dynamic Secondary Ion Mass Spectrometry Probes Distance in Lipid Assemblies: A Nanometer Chemical Ruler. *J. Am. Chem. Soc.* **2016**, *138* (51), 16737−16744.
(48) Tokumasu, F.; Jin, A. J.; Feigenson, G. W.; Dvorak, J. A. Nanoscopic Lipid Domain Dynamics Revealed by Atomic Force Microscopy. *Biophys. J.* **2003**, *84* (4), 2609−2618.
(49) Bhatia, T.; Husen, P.; Ipsen, J. H.; Bagatolli, L. A.; Simonsen, A. C. Fluid Domain Patterns in Free-Standing Membranes Captured on a Solid Support. *Biochim. Biophys. Acta BBA - Biomembr.* **2014**, *1838* (10), 2503−2510.
(50) Garg, S.; Castro-roman, F.; Porcar, L.; Butler, P.; Bautista, P. J.; Krzyzanowski, N.; Perez-salas, U. Cholesterol Solubility Limit in Lipid Membranes Probed by Small Angle Neutron Scattering and MD Simulations. *Soft Matter* **2014**, *10* (46), 9313−9317.
(51) Huang, J.; Buboltz, J. T.; Feigenson, G. W. Maximum Solubility of Cholesterol in Phosphatidylcholine and Phosphatidylethanolamine Bilayers. *Biochim. Biophys. Acta BBA - Biomembr.* **1999**, *1417* (1), 89−100.
(52) Stevens, M. M.; Honerkamp-smith, A. R.; Keller, S. L. Solubility Limits of Cholesterol, Lanosterol, Ergosterol, Stigmasterol, and β-Sitosterol in Electroformed Lipid Vesicles. *Soft Matter* **2010**, *6* (23), 5882.
(53) Kahya, N.; Scherfeld, D.; Bacia, K.; Poolman, B.; Schwille, P. Probing Lipid Mobility of Raft-Exhibiting Model Membranes by Fluorescence Correlation Spectroscopy. *J. Biol. Chem.* **2003**, *278* (30), 28109−28115.
(54) Konyakhina, T. M.; Feigenson, G. W. Phase Diagram of a Polyunsaturated Lipid Mixture: Brain Sphingomyelin/1-Stearoyl-2-Docosahexaenoyl-Sn-Glycero-3-Phosphocholine/Cholesterol. *Biochim. Biophys. Acta BBA - Biomembr.* **2016**, *1858* (1), 153−161.
(55) Boban, Z.; Mardešić, I.; Subczynski, W. K.; Jozić, D.; Raguz, M. Optimization of Giant Unilamellar Vesicle Electroformation for Phosphatidylcholine/Sphingomyelin/Cholesterol Ternary Mixtures. *Membranes* **2022**, *12* (5), 525.

https://doi.org/10.1021/jacs.3c09039
J. Am. Chem. Soc. 2023, 145, 27521−27530

Secondary Ion Mass Spectrometry of Single Giant Unilamellar Vesicles Reveals Compositional Variability

Supporting Information

Dashiel S. Grusky, Ahanjit Bhattacharya, Steven G. Boxer

Department of Chemistry, Stanford University, Stanford, California, 94305-5012, United States

Contents

Section	Page Number
1. Choice of Lipid Mixture	S3
2. Normality Verification for F-tests	S4
3. Replicate Electroformation and Gentle Hydration Samples	S5
4. Verification of Absolute Calibration Accuracy	S6
5. Ternary Monolayers	S7
6. Effect of Analysis Area on Calculated Distributions	S8
7. ^{13}C-labeled Lipid comparisons in Pure and Ternary Mixtures	S10
8. Comparison of Pure POPC Mixtures with different Methods	S11
9. Detector Counts on Bilayers and Exposed Substrate	S12
10. Correcting Ternary GUV Compositional Variability	S13
11. Nanoscale Heterogeneity in Lipid Films	S15
12. Relation between GUV Patch Size and $^{13}C_{18}$-DSPC and $^{2}H_{31}$-POPC Concentrations	S17
13. Assessing the Extent of GUV Mixing during Patch Formation	S18
14. Tracking Cholesterol Concentration in Triply Labeled Bilayers	S20
15. Assessing Average $^{2}H_{31}$-POPC Concentration in $^{13}C_{27}$-CHOL Containing Patches	S22
16. Tabulated Raw GUV Composition data	S23
17. Dot Plot Representations of GUV Composition Distributions	S28

1. Choice of Lipid Mixture

For this study, a ternary mixture with an overall composition of 40:40:20 DSPC:POPC:CHOL was used. The ternary phase diagram for this mixture is shown in Figure S1. Measurements for this diagram were made at 23°C. This mixture was chosen because it is well-studied in GUVs[1] and in bilayer patches formed from GUVs on SiO_2[2,3]. Additionally, since the mixture does not display macroscopic phase separation within the 50nm lateral resolution of the NanoSIMS, bilayer patches formed from GUVs appear uniform, simplifying quantitative analysis. It should be noted that although macroscopic domain formation is not apparent, nanoscale domain formation has been documented in this mixture using methods that surpass both the optical diffraction limit and the lateral resolution of the NanoSIMS[1–3]. Note that such phase diagrams are based on the assumption that the composition of GUVs match the nominal composition of the components dissolved in organic solvents prior to GUV formation. Note that while the nominal composition is placed within the $L_d + L_o$ coexistence region of the diagram (denoted by the red star in figure S1). As a result, some GUVs may contain some degree of solid Lβ, which although not visible via NanoSIMS, may still be present and have implications for GUV deposition, and corresponding compositional variability.

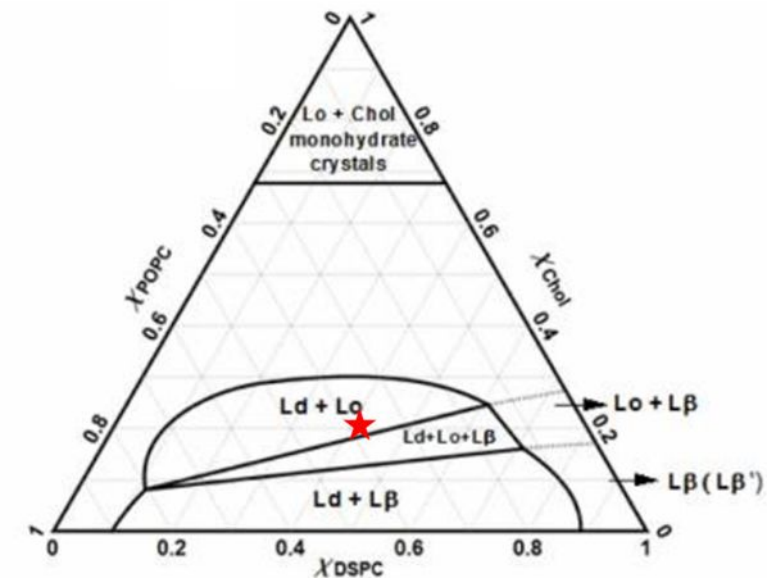

Figure S1. DSPC/POPC/CHOL ternary phase diagram. The phase diagram for the ternary DSPC/POPC/CHOL mixture is adapted from ref. 1 (Konyakhina, T. M.; Wu, J.; Mastroianni, J. D.; Heberle, F. A.; Feigenson, G. W. Phase Diagram of a 4-Component Lipid Mixture: DSPC/DOPC/POPC/Chol. *Biochim. Biophys. Acta BBA - Biomembr.* **2013**, *1828* (9), 2204–2214). The red star denotes the nominal position of the mixture used in this study (40 : 40 : 20 DSPC : POPC : CHOL).

2. Normality Verification for F-tests

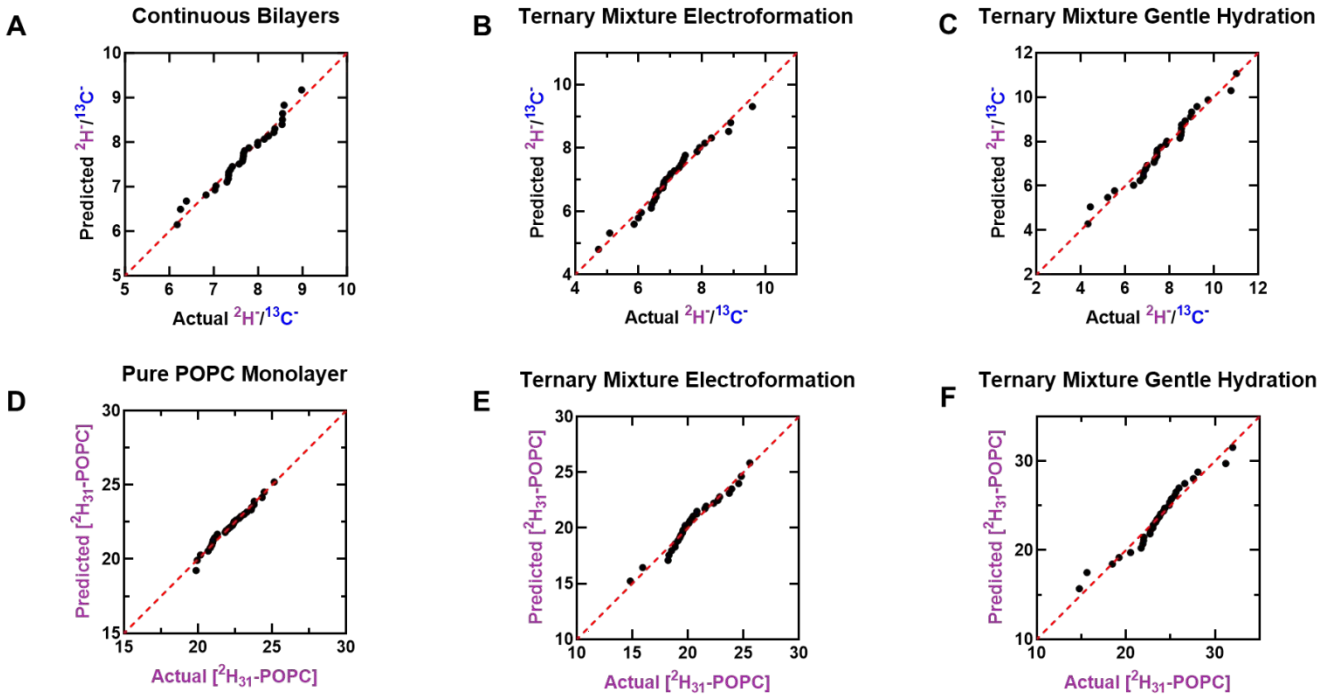

Figure S2. Sample QQ-plots for ternary and pure POPC mixtures. (A-C) QQ-plots of the measured $^{2}H^{-}/^{13}C^{-}$ ratios shown in Figure 4 of the main text. (D-E) QQ-plots of the measured $^{2}H_{31}$-POPC concentrations shown in Figure 5D of the main text. For all plots, the red dashed line represents the identity line.

Data compared via F-test were assessed for normality, as a fundamental assumption of F-tests is that the data examined should be normally distributed. The normality of a given distribution can be examined via quantile-quantile plots (QQ-plots), which plot experimental values against predicted values assuming a normal distribution. Several sample QQ-plots can be seen in Figure S2, and they display a linear relationship between actual and predicted values, indicating that the data are normally distributed. Plots were made for all samples, with the majority being highly linear, similar to the sample plots shown in Figure S2. The only distribution with visible deviation from linearity in the QQ-plot is the $^{13}C_{18}$-DSPC concentration distribution (See figure 5B) for ternary DSPC/POPC/CHOL GUVs formed via gentle hydration. The plot for this distribution can be seen in Figure S3, which suggests that the distribution is

somewhat right skewed. It should therefore be noted that the application of an F-test to this distribution may be less valid than for the remaining data sets.

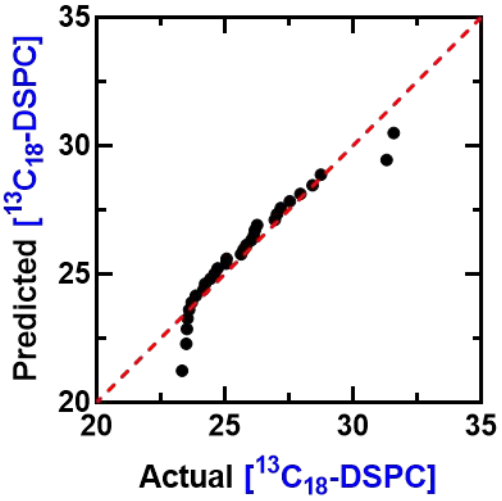

Figure S3. QQ-plot for $^{13}C_{18}$-DSPC concentrations of ternary bilayer patches formed via gentle hydration. Data for this plot are taken from Figure 5B of the main text. Bilayer patches with lower measured concentrations of $^{13}C_{18}$-DSPC fall below the identity line, suggesting a slight right skew in the data.

3. Replicate Electroformation and Gentle Hydration Samples

Replicate electroformation and gentle hydration samples were examined to see if the difference in variability between the two methods was reproducible. The results from these replicate samples can be seen in Figure S4. These samples were produced using the same master stock as the samples shown in Figure 4 of the main text. Relative concentration changes were assessed via the $^{2}H^{-}/^{13}C^{-}$ ratio, which again demonstrated significantly less variability in electroformed GUV patches. Absolute concentration quantification via external calibration curves showed that the $^{2}H_{31}$-POPC concentration was also more homogenous in electroformed GUV patches, although the $^{13}C_{18}$-DSPC concentration did not display a significant difference in variability between the two methods.

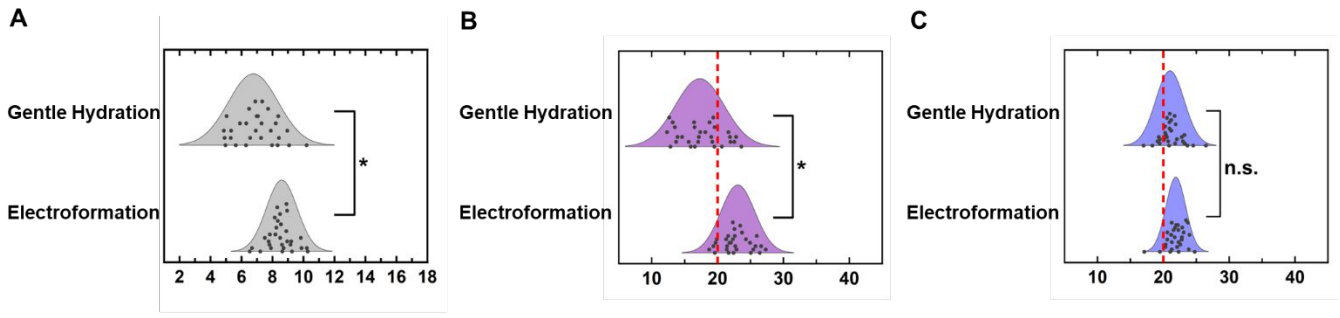

D

Method	$^{2}H^{-}/^{13}C^{-}$ Ratio Standard Deviation	[$^{13}C_{18}$-DSPC] Standard Deviation	[$^{2}H_{31}$-POPC] Standard Deviation
Gentle Hydration	1.5	1.9	3.4
Electroformation	0.9	1.5	2.3

Figure S4. Replicate gentle hydration and electroformation samples. Electroformation and gentle hydration samples were compared via (A) $^{2}H^{-}/^{13}C^{-}$ ratio, (B) $^{13}C_{18}$-DSPC concentration, and (C) $^{2}H_{31}$-POPC concentration. Dot plot representations of these distributions can be seen in Figure S24. (D) Calculated standard deviations for the distributions in (A)-(C).

4. Verification of Absolute Calibration Accuracy

The accuracy of the external calibration curves for $^{13}C_{18}$-POPC and $^{13}C_{18}$-DSPC was estimated by comparing measured $^{13}C^{-}/(^{13}C^{-} + {}^{12}C^{-})$ ion ratios to expected ratios. Expected ratios were calculated by determining the number of ^{13}C and ^{12}C carbons present in a sample. For example, in a sample containing 10 mol % $^{13}C_{18}$-POPC (remainder being natural abundance POPC), out of 100 lipid molecules 10 of them are $^{13}C_{18}$-POPC, leading to a total of 180 intentionally ^{13}C-labeled carbons. Additionally, 1.1% of the remaining carbons will be ^{13}C at natural abundance, adding another 44.2 ^{13}C carbons. Dividing 224.2 by the total number of carbons (4200), yields the predicted $^{13}C^{-}/(^{13}C^{-} + {}^{12}C^{-})$ ion ratio of 0.0533. These calculations were carried out for calibration curves containing varying concentrations of $^{13}C_{18}$-POPC and $^{13}C_{18}$-DSPC with the resulting values tabulated next to experimental values in Figure S5. Figure S5 demonstrates that there is reasonable agreement between the predicted values and the experimental data.

A

Mole Percent $^{13}C_{18}$-POPC	Predicted $^{13}C^-/(^{13}C^- + ^{12}C^-)$	Measured $^{13}C^-/(^{13}C^- + ^{12}C^-)$
0	0.011	0.0169
10	0.0533	0.0510
20	0.0957	0.0840
30	0.1380	0.1262
40	0.1803	0.1513
50	0.2226	0.1830

B

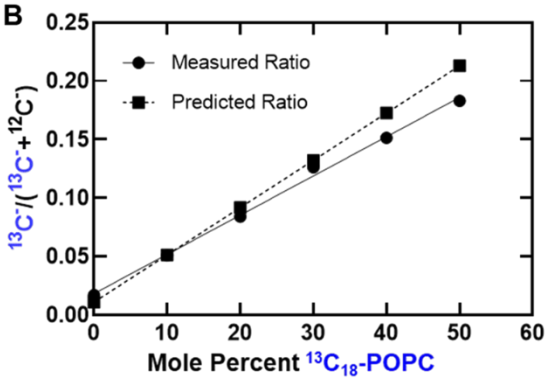

C

Mole Percent $^{13}C_{18}$-DSPC	Predicted $^{13}C^-/(^{13}C^- + ^{12}C^-)$	Measured $^{13}C^-/(^{13}C^- + ^{12}C^-)$
0	0.011	0.0169
10	0.0514	0.0619
20	0.0918	0.0905
30	0.1322	0.1227
40	0.1726	0.1550
50	0.213	0.1911

D

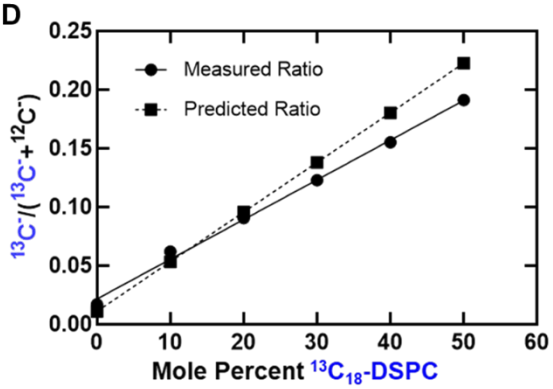

Figure S5. Calibration curve accuracy verification. Comparison of calculated $^{13}C^-/(^{13}C^- + ^{12}C^-)$ ratios and experimental ratios (from standard samples) for $^{13}C_{18}$-POPC (A and B) and $^{13}C_{18}$-DSPC (C and D). Standard samples were made by spreading a mixture with the indicated concentration of labeled lipid (remaining is corresponding natural abundance lipid) on patterned NanoSIMS substrates. The linear fits in panels B and D correspond to the measured ratios using standard samples.

5. Ternary Monolayers

Ternary monolayers made using the $^{13}C_{18}$-DSPC and $^{2}H_{31}$-POPC ternary master stock were formed on a LB trough as described in the materials and methods. The advantage of examining a ternary monolayer with this composition is that it could be more homogenous than a GUV sample and it would have the same anti-correlation between ^{13}C- and ^{2}H-labeled lipids as the GUV samples analyzed in Figure 3 and 4 of the main text. This would allow for the ternary monolayer to be compared to the GUV samples via the $^{2}H^-/^{13}C^-$ ratio. However, this comparison was not made due to macroscale separation present in ternary monolayers with this composition, as can be seen in Figure S6. This separation between saturated and unsaturated lipids is likely due to the fact that these monolayers are not heated while being produced and therefore do not allow for significant mixing between lipids. Due to this macroscale separation, the measured $^{2}H^-/^{13}C^-$ ratio will depend heavily on the relative area occupied by the POPC and DSPC rich regions within a given

analysis region. Due to this confounding variable, a direct comparison between ternary monolayers and ternary GUVs was not made.

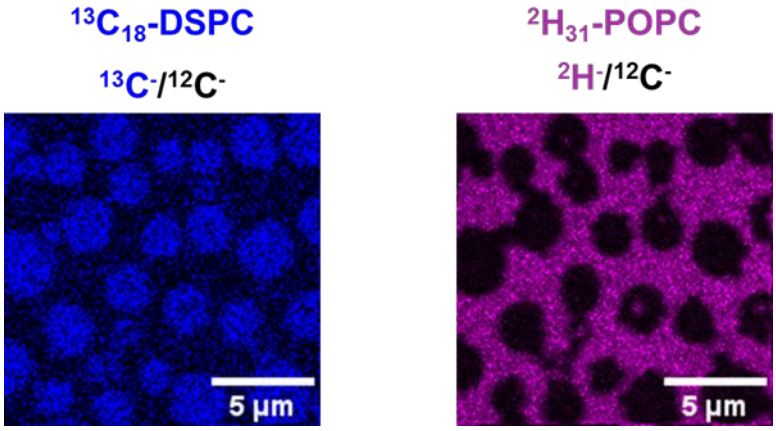

Figure S6. NanoSIMS images of ternary monolayers. Ion Images of a ternary monolayer containing $^{13}C_{18}$-DSPC and $^{2}H_{31}$-POPC. As can be seen in the images, $^{13}C_{18}$-DSPC and $^{2}H_{31}$-POPC are macroscopically separated.

6. Effect of Analysis Area on Calculated Distributions

A potential concern with the methodology presented here is that smaller GUV patches may have intrinsically lower signal to noise. To assess if the size of a given GUV patch, and therefore the size of the region analyzed, influences the resulting concentration distributions, the gentle hydration and electroformation samples discussed in Figures 4 and 5 of the main text were further investigated. GUV patches were re-analyzed using a fixed region of interest so that any effect due to the size of analysis region on the resulting measurements is controlled for. A 30x30 pixel region of interest (2.9x2.9 µm) was defined for each GUV patch and the corresponding $^{2}H^-/^{13}C^-$ ratios as well as $^{2}H_{31}$-POPC and $^{13}C_{18}$-DSPC concentrations were calculated (the latter two used the same set of calibration curves shown in Figure 5 of the main text to determine labeled lipid concentrations) within this region. This was done for each of the GUV patches analyzed in Figures 4 and 5 of the main text. The resulting fixed area distributions were then compared to the distributions calculated using the whole GUV patch (the same distributions shown in Figures 4 and 5 of the main text), with the results shown in Figure S7. For GUV patches formed by either gentle hydration or electroformation, there is not a significant difference (determined via F-test) between distributions calculated using the full GUV patch and those calculated using the fixed 2.9x2.9 µm region of interest. This suggests that the total area selected for $^{2}H^-/^{13}C^-$ and labeled lipid concentration analysis does not have a significant impact on the measured distributions and their corresponding variability. However, there is a consistent increase in the standard deviations of distributions calculated with the fixed area

analysis relative to those where the full patch was used (Figure S7 G and H). Although this change is not statistically significant, it does suggest that using smaller analysis regions typically leads to slight increases in variability. This is presumably due to smaller analysis regions having less signal. GUV patches formed by either gentle hydration or electroformation were further compared using the fixed area method as shown in Figure S8. The fixed area method recapitulates the result that GUVs formed via electroformation have less compositional variability than those formed via gentle hydration. This is evident using both relative changes in labeled lipid concentration ($^{2}H^{-}/^{13}C^{-}$ ratio) and absolute labeled lipid concentrations ($^{13}C_{18}$-DSPC and $^{2}H_{31}$-POPC concentrations).

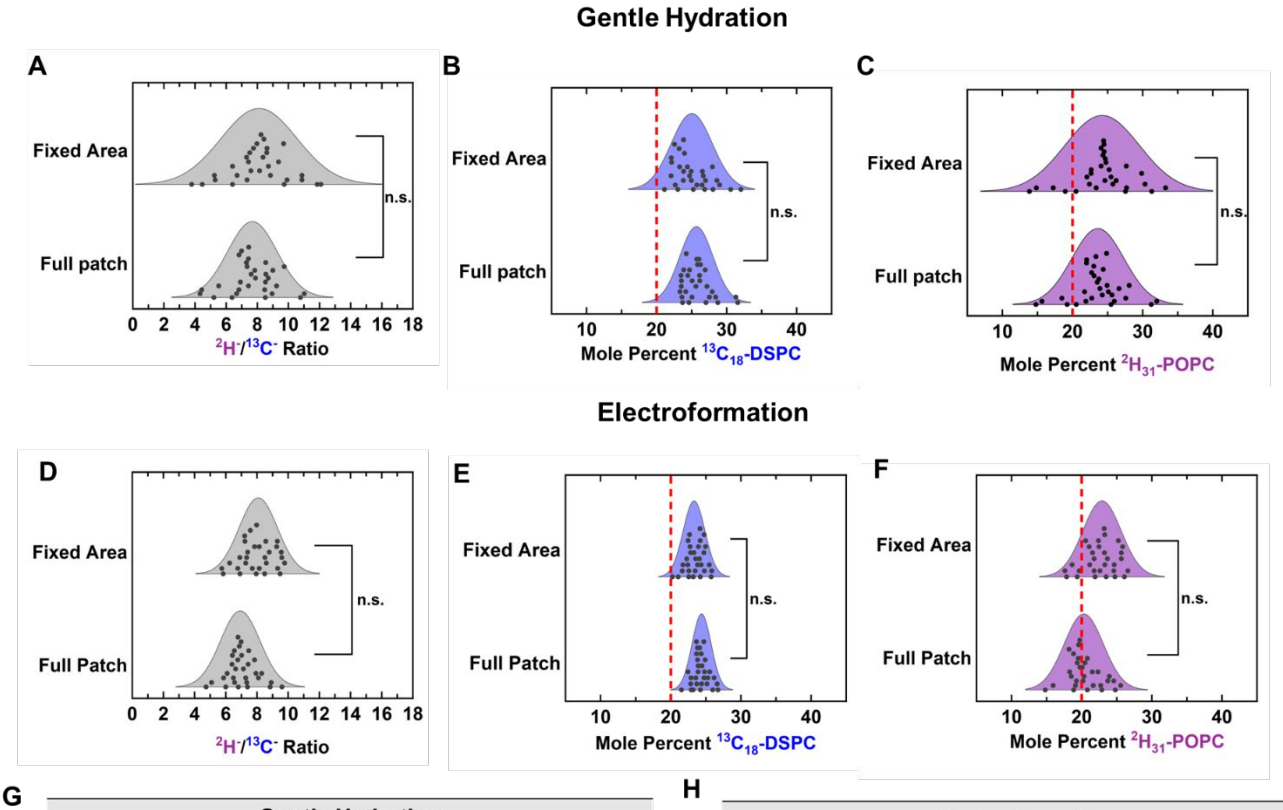

G

Gentle Hydration			
Analysis Method	$^{2}H^{-}/^{13}C^{-}$ Ratio Standard Deviation	[$^{13}C_{18}$-DSPC] Standard Deviation	[$^{2}H_{31}$-POPC] Standard Deviation
Fixed Area	2.0	2.7	4.3
Full Patch	1.6	2.2	3.7

H

Electroformation			
Analysis Method	$^{2}H^{-}/^{13}C^{-}$ Ratio Standard Deviation	[$^{13}C_{18}$-DSPC] Standard Deviation	[$^{2}H_{31}$-POPC] Standard Deviation
Fixed Area	1.1	1.4	2.5
Full Patch	1.1	1.2	2.6

Figure S7. Effect of analysis area on measured distributions. $^{2}H^{-}/^{13}C^{-}$ ratios, $^{13}C_{18}$-DSPC concentrations and $^{2}H_{31}$-POPC concentrations were determined within a fixed 30x30 pixel region (2.9x2.9 μm). This analysis was performed on the same GUV patches analyzed in Figures 4 and 5 of the main text. The distributions calculated using a fixed area are plotted next to distributions calculated for the same GUV patches but using their full area. The resulting distributions for GUVs made via gentle hydration (A-C) and electroformation (D-F), with corresponding standard deviations seen in (G) and (H) are displayed. The variability in the distributions remained the same (determined via F-test) regardless of which analysis method was used. Dot plot representations of these distributions can be seen in Figure S25.

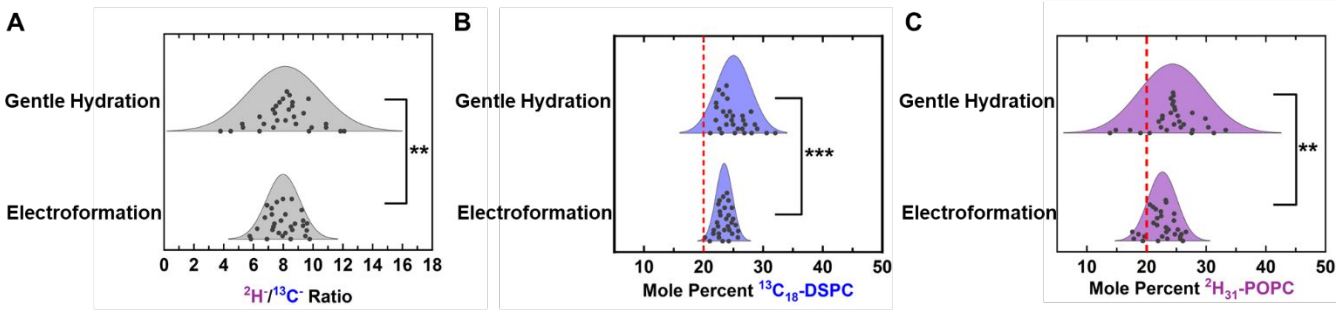

D

Method	$^{2}H^{-}/^{13}C^{-}$ Ratio Standard Deviation	[$^{13}C_{18}$-DSPC] Standard Deviation	[$^{2}H_{31}$-POPC] Standard Deviation
Gentle Hydration	2.0	2.7	4.3
Electroformation	1.1	1.4	2.5

Figure S8. Comparison of different methods using fixed analysis area. GUV patches formed via gentle hydration and electroformation (same sample and patches from Figures 4 and 5 of the main text) had their $^{2}H^{-}/^{13}C^{-}$ ratios, $^{13}C_{18}$-DSPC concentrations and $^{2}H_{31}$-POPC concentrations calculated within a fixed 30x30 pixel area (2.9x2.9 μm). The calculated $^{2}H^{-}/^{13}C^{-}$ ratio and concentration distributions are compared for each method (A-C) with the corresponding standard deviations shown in (D). Dot plot representations of these distributions can be seen in Figure S26.

7. ^{13}C-labeled Lipid Comparisons in Pure and Ternary Mixtures

A pure POPC mixture ($^{13}C_{18}$-POPC:$^{2}H_{31}$-POPC:POPC 20:20:60) was used to form GUVs either via electroformation or gentle hydration. In addition to comparing $^{2}H_{31}$-POPC concentration variability in the pure POPC sample to that of the ternary mixture (Figure 6 of the main text) the concentration variability of the $^{13}C_{18}$-labeled lipid ($^{13}C_{18}$-POPC for the pure POPC sample and $^{13}C_{18}$-DSPC in the ternary mixture) was also compared. This comparison can be seen in Figure S9 for GUVs formed via gentle hydration and electroformation. In both cases, the pure POPC sample displayed significantly less variability, recapitulating the results in Figure 6 of the main text.

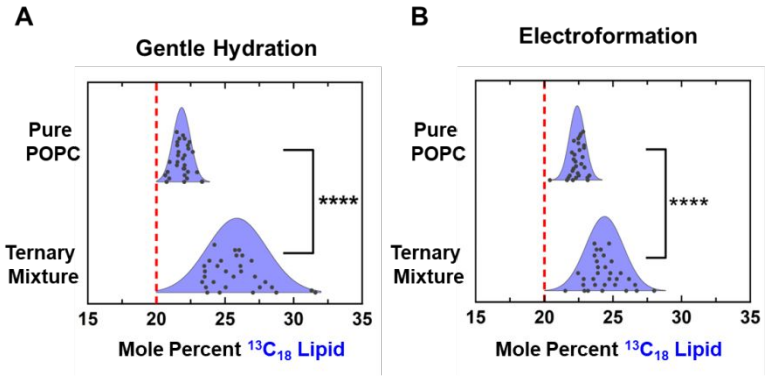

C

Method	[$^{13}C_{18}$ Lipid] Standard Deviation	
	Pure POPC	Ternary Mixture
Gentle Hydration	0.6	2.2
Electroformation	0.6	1.2

Figure S9. ^{13}C-labeled lipid concentrations in pure POPC and ternary mixtures. ^{13}C-lipid concentration comparisons between pure and ternary mixtures formed by gentle hydration (A) or electroformation (B). For the pure POPC sample, the ^{13}C-labeled lipid is $^{13}C_{18}$-POPC, whereas for the ternary mixture, $^{13}C_{18}$-DSPC is the ^{13}C-labeled lipid. Dot plot representations of these distributions can be seen in Figure S27. (C) Standard deviations for the distributions shown in (A) and (B).

8. Comparison of Pure POPC Mixtures with different Methods

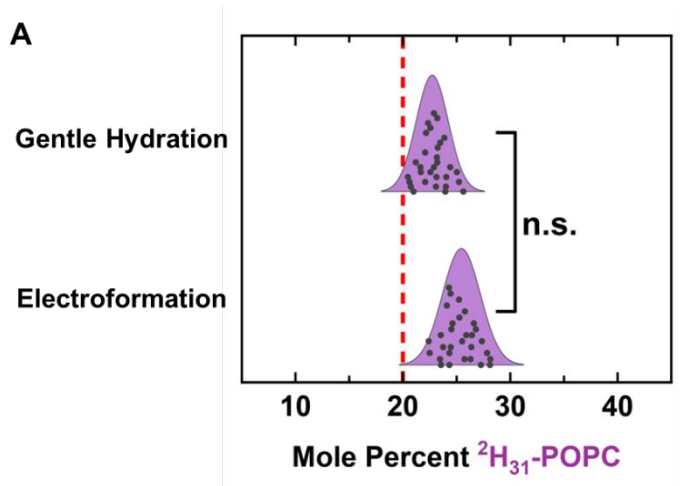

B

Method	[$^{2}H_{31}$-POPC] Standard Deviation
Gentle Hydration	1.4
Electroformation	1.6

Figure S10. $^{2}H_{31}$-POPC concentrations in pure POPC samples. $^{2}H_{31}$-POPC concentrations were compared between samples formed either by electroformation or gentle hydration. The resulting $^{2}H_{31}$-POPC concentrations distributions can be seen in (A) and the corresponding standard deviations can be seen in (B). Dot plot representations of these distributions can be seen in Figure S28.

The variability in pure POPC samples ($^{13}C_{18}$-POPC:$^{2}H_{31}$-POPC:POPC 20:20:60) was examined for patches formed via electroformation and gentle hydration. As seen in Figure S10, the $^{2}H_{31}$-POPC concentration variability is not significantly different between the two methods as assessed via F-test. This

suggest that the methods themselves do not have significant differences in terms of surface contamination, and that any difference in variability between gentle hydration and electroformation in ternary mixtures is not the result of one method being more prone to contamination of GUVs or systematic error in the NanoSIMS analysis. Instead, the differences in variability are due to the method of GUV preparation itself.

9. Detector Counts on Bilayers and Exposed Substrate

To further explore if significant contamination is present on the surfaces on which bilayers were deposited, the raw ion counts on several detectors were examined. 30x30 pixel (2.9x2.9 μm) regions of interest (ROIs) were defined either on exposed substrate or on bilayer patches. For at least 23 ROIs on either bilayer or exposed substrate, the total counts on the detectors set to $^{2}H^{-}$, $^{13}C^{-}$ and $^{12}C^{-}$ were determined and then averaged. This analysis was done for GUV patches containing $^{13}C_{18}$-DSPC and $^{2}H_{31}$-POPC. GUV patches formed via gentle hydration or electroformation were analyzed (data taken from the same patches discussed in Figures 4 and 5 of the main text), with the results displayed in Figure S11. For all detectors, average counts were significantly higher in regions containing bilayer than those without bilayer (assessed via t-test). This suggests that there is minimal contamination of the surface, particularly for $^{2}H^{-}$ and $^{13}C^{-}$, which have 32 and 9 times more counts on bilayer than on exposed substrate respectively. $^{12}C^{-}$ counts on a bilayer are only three times higher those on exposed substrate, suggesting some level of ^{12}C is deposited on the surface even where there is not bilayer present, which is the major limitation of the absolute quantification method detailed in the main text. However, the $^{12}C^{-}$ counts appear to be consistent from sample to sample, as the raw $^{12}C^{-}$ counts on exposed substrate are similar between the exposed gentle hydration and electroformation substrates. Additionally, as suggested by Figure 6, Figure S9, and Figure S10, sample contamination alone cannot explain the large variability seen in labeled lipid concentrations of ternary samples. This suggests that while there is $^{12}C^{-}$ background, this background is relatively constant from sample to sample and not a major factor driving the observed variability in ternary mixtures. Additionally, it should be noted that although the natural abundance of $^{13}C^{-}$ is 1.1%, the average $^{13}C^{-}/(^{13}C^{-} + ^{12}C^{-})$ ratio on regions without bilayer is 0.039 and 0.024 for gentle hydration and electroformation respectively. This corresponds to 3.9% and 2.4% of the carbon background on the substrate being labeled. This suggests that some debris is deposited on the substrate, presumably during the rupturing and freeze-drying process, leading to ^{13}C enrichment on the substrate from ^{13}C-labeled lipids.

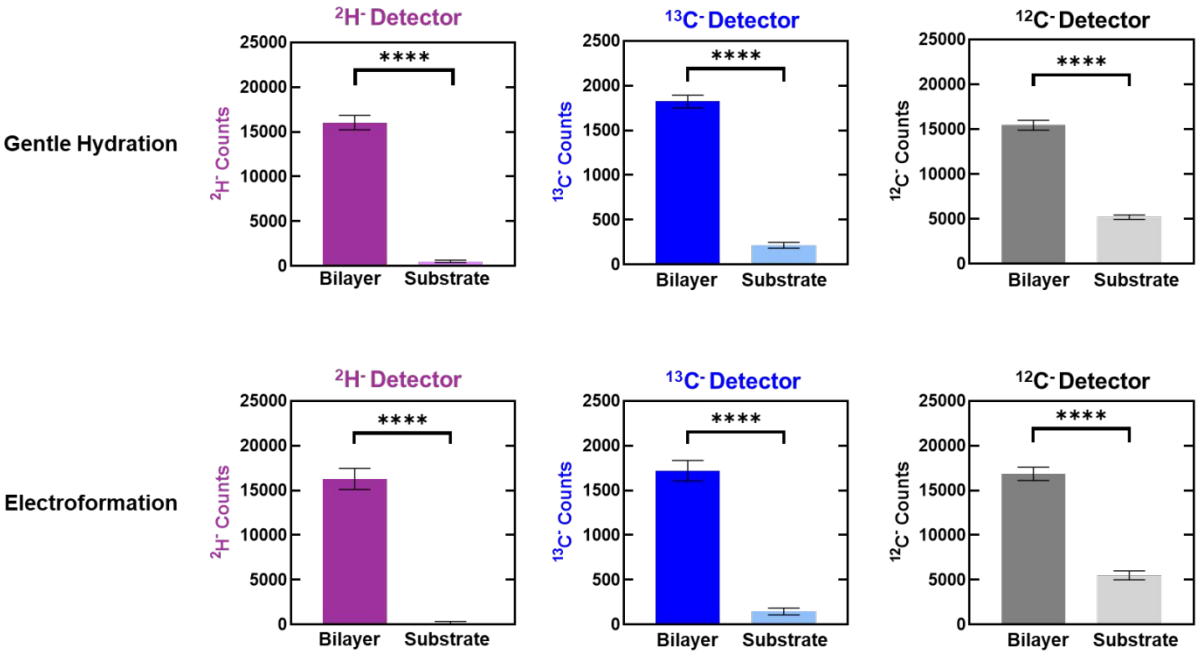

Figure S11. Comparison of detector counts on bilayer and exposed substrate. Raw counts on detectors set to $^{2}H^{-}$, $^{13}C^{-}$ and $^{12}C^{-}$ were compared between regions of interest on bilayer and on exposed substrate. The top row displays counts on each detector for bilayer patches formed from GUVs via gentle hydration and regions on the same sample where the substrate is exposed (no bilayer present). The bottom row displays the equivalent data collected from an electroformation sample. Both samples had the same nominal lipid composition (DSPC:$^{13}C_{18}$-DSPC:POPC:$^{2}H_{31}$-POPC:CHOL 20:20:20:20:20) and were drawn from the same master stock.

10. Correcting Ternary GUV Compositional Variability

In order to approximate the absolute compositional variability (excluding variability resulting from sample preparation and NanoSIMS analysis), the standard deviations of ternary GUVs formed via electroformation or gentle hydration were corrected using several different methods. The expression used to correct the ternary samples can be seen in figure S12A, where the observed ternary standard deviations are adjusted using the standard deviations from different control samples. The standard deviations from four different control samples were used as proxies for the variability due to sample preparation and instrumentation: continuous bilayers formed via rupture of 100nm diameter extruded ternary SUVs, monolayers composed of pure POPC with 20 mol % $^{2}H_{31}$-POPC and GUVs with the sample pure POPC composition formed via either gentle hydration or electroformation. The first sample can be used as a proxy for the variability in sample preparation and analysis for $^{2}H^{-}/^{13}C^{-}$ ratio, as well as $^{13}C_{18}$-DSPC and $^{2}H_{31}$-POPC concentrations. Continuous bilayers formed from SUVs should be more compositionally homogenous than individual GUV patches, as each bilayer within a corral of a NanoSIMS substrate is

formed from the rupture of hundreds of SUVs, and therefore should represent the average composition more accurately. This can be seen in Figure S12B, where the variability in ternary SLBs formed from extruded SUVs is consistently lower than variability in ternary GUV patches formed via either gentle hydration or electroformation. Correcting the standard deviations of the ternary GUV samples using the ternary SUV bilayers yields the table shown in Figure S12C. However, since the preparation of continuous bilayers is not identical to that of bilayer patches, additional corrections were performed using pure POPC samples ($^{2}H_{31}$-POPC:$^{13}C_{18}$-POPC:POPC 20:20:60). Since these samples have only one lipid component, they are expected to be far more uniform. Additionally, pure POPC samples formed via electroformation and gentle hydration have the same sample preparation protocol as their corresponding ternary mixtures, and therefore are better at approximating the variability inherent to sample preparation. However, these samples can only be compared via their $^{2}H_{31}$-POPC concentrations, as they do not contain $^{13}C_{18}$-DSPC, and the corresponding $^{2}H^{-}/^{13}C^{-}$ ratio is not comparable between pure and ternary mixtures (Figure 3 of the main text). Corrections were also performed using pure POPC monolayers, which may be the best approximation for instrument variability, given that they should be essentially homogenous. However, since monolayers have distinctly different sample preparation from GUV patches, correcting ternary GUV patch variability with pure POPC monolayer variability does not account for variation introduced from sample preparation. The corrections to $^{2}H_{31}$-POPC concentration variability can be seen in figure S12D and are similar regardless of which pure POPC sample is used. The results in Figures S12C and D can be taken as approximations of GUV variability due to composition and method, rather than variability from sample preparation and NanoSIMS analysis. It should also be noted that since the measured variability in $^{2}H_{31}$-POPC concentrations in continuous bilayers produced from ternary SUVs is nearly identical to that of the other pure POPC samples, the covariance between sample preparation, instrument noise and the observed variability is likely minimal (ternary mixtures do not have inherently higher variation due to sample preparation or instrumentation).

A

$$(\sigma_{observed})^2 = (\sigma_{instrument})^2 + (\sigma_{sample\ prep})^2 + (\sigma_{formation\ method})^2$$

$$\sigma_{formation\ method} = \sqrt{(\sigma_{observed})^2 - (\sigma_{instrument})^2 - (\sigma_{sample\ prep})^2}$$

Ternary Mixture

Approximated with control samples

B

Uncorrected Standard Deviations			
Sample	$^2H^-/^{13}C^-$ Ratio Standard Deviation	[$^{13}C_{18}$-DSPC] Standard Deviation	[$^2H_{31}$-POPC] Standard Deviation
Ternary Gentle Hydration	1.6	2.2	3.7
Ternary Gentle Hydration Replicate	1.5	1.9	3.4
Ternary Electroformation	1.1	1.2	2.6
Ternary Electroformation Replicate	1.1	1.4	2.5
Continuous Bilayer	0.7	1.0	1.4
Pure POPC monolayer	n/a	n/a	1.4
Pure POPC Gentle Hydration	n/a	n/a	1.4
Pure POPC Electroformation	n/a	n/a	1.6

C

Standard Deviations Corrected with Continuous Bilayer			
Corrected Sample	$^2H^-/^{13}C^-$ Ratio Standard Deviation	[$^{13}C_{18}$-DSPC] Standard Deviation	[$^2H_{31}$-POPC] Standard Deviation
Ternary Gentle Hydration	1.4	1.9	3.5
Ternary Gentle Hydration Replicate	1.3	1.6	3.1
Ternary Electroformation	0.8	0.7	2.2
Ternary Electroformation Replicate	0.9	1.0	2.1

D

Corrected [$^2H_{31}$-POPC] Standard Deviations			
	Sample used for correction		
Corrected Sample	Pure POPC monolayer	Pure POPC Gentle Hydration	Pure POPC Electroformation
Ternary Gentle Hydration	3.5	3.5	3.4
Ternary Gentle Hydration Replicate	3.1	3.1	3.0
Ternary Electroformation	2.2	2.2	2.0
Ternary Electroformation Replicate	2.1	2.1	1.9

Figure S12. Corrected standard deviations of ternary GUVs. (A) Expression for sources of error and the rearrangement used to performed corrections. (B) Uncorrected standard deviations from GUV, SUV and monolayer samples. (C) Corrected standard deviations for GUV patches formed via gentle hydration and electroformation. GUV Standard deviations were corrected using the standard deviation for continuous bilayers formed from extruded SUVs shown in (B). (D) Corrected $^2H_{31}$-POPC concentrations in ternary GUV patches formed via gentle hydration or electroformation. Standard deviations were corrected using the values listed in (B) for the corresponding pure POPC sample.

11. Nanoscale Heterogeneity in Lipid Films

Since GUVs are produced from a dried down lipid film, one possible source of GUV heterogeneity is the lipid film itself. Lipids films made from the ternary master stock containing $^{13}C_{18}$-DSPC and $^2H_{31}$-POPC were examined for macroscale separation. As can be seen in Figure S13, there is no resolvable macroscopic separation between $^{13}C_{18}$-DSPC and $^2H_{31}$-POPC within the ternary film. The NanoSIMS 50L has a 50nm lateral resolution limit, so it is possible that preferential interactions between lipids within the film take place over a smaller length scale. To address this possibility, recombination between $^{13}C^-$ and $^2H^-$ to form triply labeled acetylide ($^{13}C_2{}^2H^-$) was examined. When a sample containing ^{13}C- and ^2H-labels on different lipids is rastered by the primary Cs^+, secondary $^{13}C^-$ and $^2H^-$ ions are ejected and then recombine to form $^{13}C_2{}^2H^-$ (figure S14A and B). This method, which has be examined in detail previously with $^{13}C^{15}N^-$ or $^{13}C_2{}^2H^-$ recombinant ions[2–4], is sensitive to the average distance between the two different isotopic labels on the order of 1-3nm. The recombination ratio, $\Re(^{13}C_2{}^2H^-) = {}^{13}C_2{}^2H^-/(^{13}C_2{}^2H^- + {}^{13}C_2H^- + {}^{12}C_2{}^2H^-)$ for a ternary film containing $^{13}C_{18}$-DSPC and $^2H_{31}$-POPC can be compared to the $\Re(^{13}C_2{}^2H^-)$ for a ternary film

containing $^{13}C_{18}$-POPC and $^{2}H_{31}$-POPC. This comparison provides information on which pair of labeled lipids is closer together on average. A higher $\Re(^{13}C_2{}^2H^-)$ corresponds to a smaller average distance between the differently labeled lipids, while a lower $\Re(^{13}C_2{}^2H^-)$ corresponds to a larger average distance between the differently labeled lipids. As can be seen in Figure S14C, the measured $\Re(^{13}C_2{}^2H^-)$ in films containing $^{13}C_{18}$- and $^{2}H_{31}$-POPC is higher than that of films containing $^{13}C_{18}$-DSPC and $^{2}H_{31}$-POPC (assessed via t-test). This suggests that, on the nanoscale, the two differently labeled POPC lipids are closer together on average than labeled DSPC and POPC. Although this may not be the source of the observed GUV heterogeneity, it provides a possible explanation for the correlations observed in Figure 3 of the main text. POPC lipids interact strongly with each other relative to POPC and DSPC, which is presumably why $^{13}C_{18}$-POPC and $^{2}H_{31}$-POPC are correlated, while $^{13}C_{18}$-DSPC and $^{2}H_{31}$-POPC are anti-correlated.

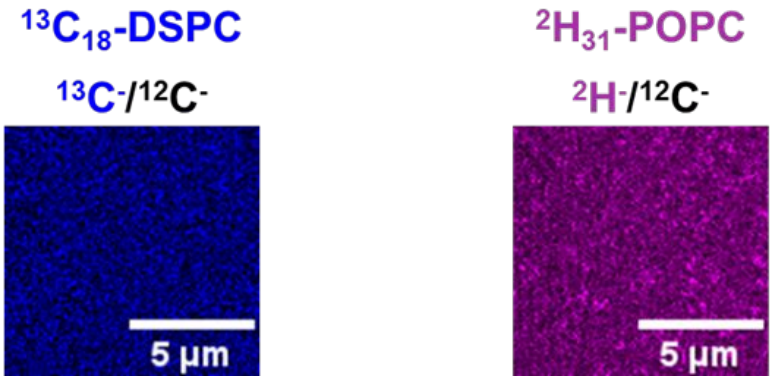

Figure S13. Lipid films are macroscopically homogenous. Representative NanoSIMS images of ternary films spread on Si/SiO_2. $^{13}C^-$ and $^{2}H^-$ secondary ions originating from $^{13}C_{18}$-DSPC and $^{2}H_{31}$-POPC respectively both appear to be homogenous.

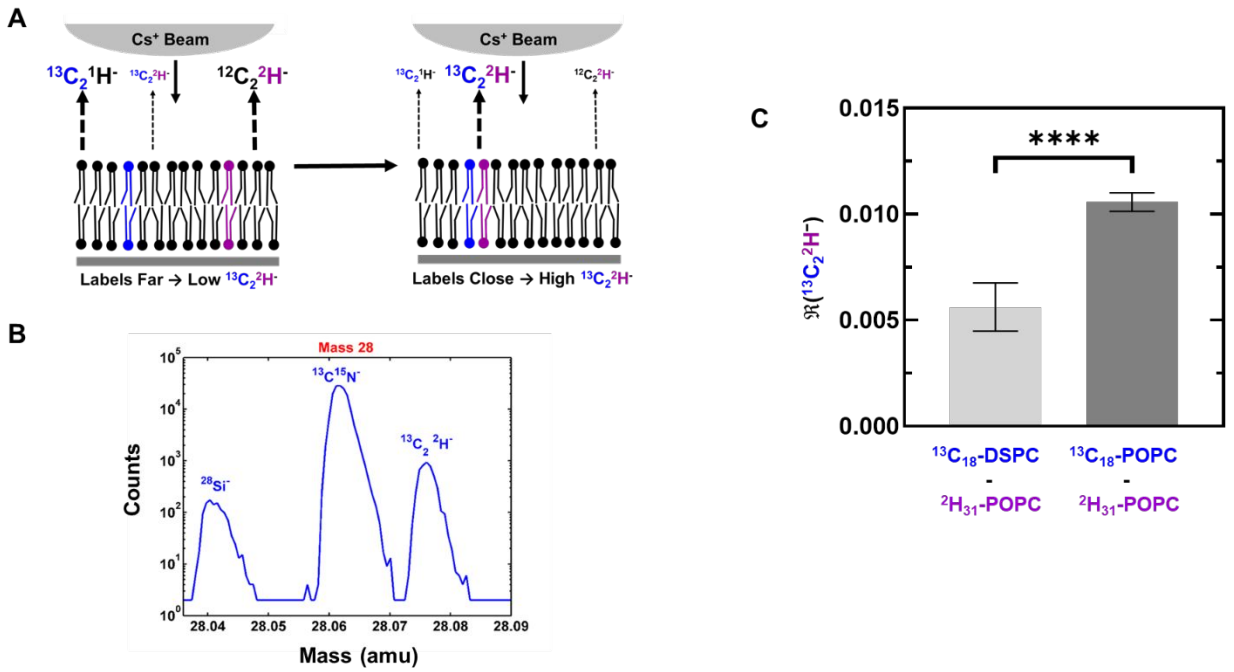

Figure S14. Acetylide recombination in lipid films. (A) Schematic describing recombination to form acetylide in lipid bilayers. When two differently labeled lipids are closer together on average, more $^{13}C_2{}^2H^-$ is formed. (B) Mass scan for mass 28 displaying good separation between triply labeled acetylide ion and any interfering isobars. Figures (A) and (B) are reproduced with permission from ref 3 (Grusky, D. S.; Moss, F. R.; Boxer, S. G. Recombination between ^{13}C and ^2H to Form Acetylide ($^{13}C_2{}^2H^-$) Probes Nanoscale Interactions in Lipid Bilayers via Dynamic Secondary Ion Mass Spectrometry: Cholesterol and GM_1 Clustering. *Anal. Chem.* **2022**, *94* (27), 9750–9757.) (C) Acetylide recombination is significantly higher in lipid films containing $^{13}C_{18}$-POPC and $^2H_{31}$-POPC relative to those containing $^{13}C_{18}$-DSPC and $^2H_{31}$-POPC. Error bars display 95% confidence intervals calculated from 9 different corrals containing lipid film.

12. Relation between GUV Patch Size and $^{13}C_{18}$-DSPC and $^2H_{31}$-POPC Concentrations

In order to assess other possible sources of GUV variability, the relationship between patch area and the measured concentrations of $^2H_{31}$-POPC and $^{13}C_{18}$-DSPC was assessed. Ternary GUV patches that could fit entirely into the 25x25 μm^2 raster were analyzed and their $^2H_{31}$-POPC and $^{13}C_{18}$-DSPC concentration determined via external calibration curves. This method was applied to ten GUV patches formed via gentle hydration (Figure S15 A-B) or electroformation (Figure S15 C-D) with no correlation seen between patch area and labeled lipid concentrations. This suggests that there is minimal effect of patch area on the resulting labeled lipid concentrations. However, it should be noted that this analysis is restricted to GUVs that can fit within the analysis region and may not apply to larger GUVs. Additionally, since the

history of each GUV patch is not known, the area of a given patch may not be a direct reflection of the size of GUV that produced the observed patch.

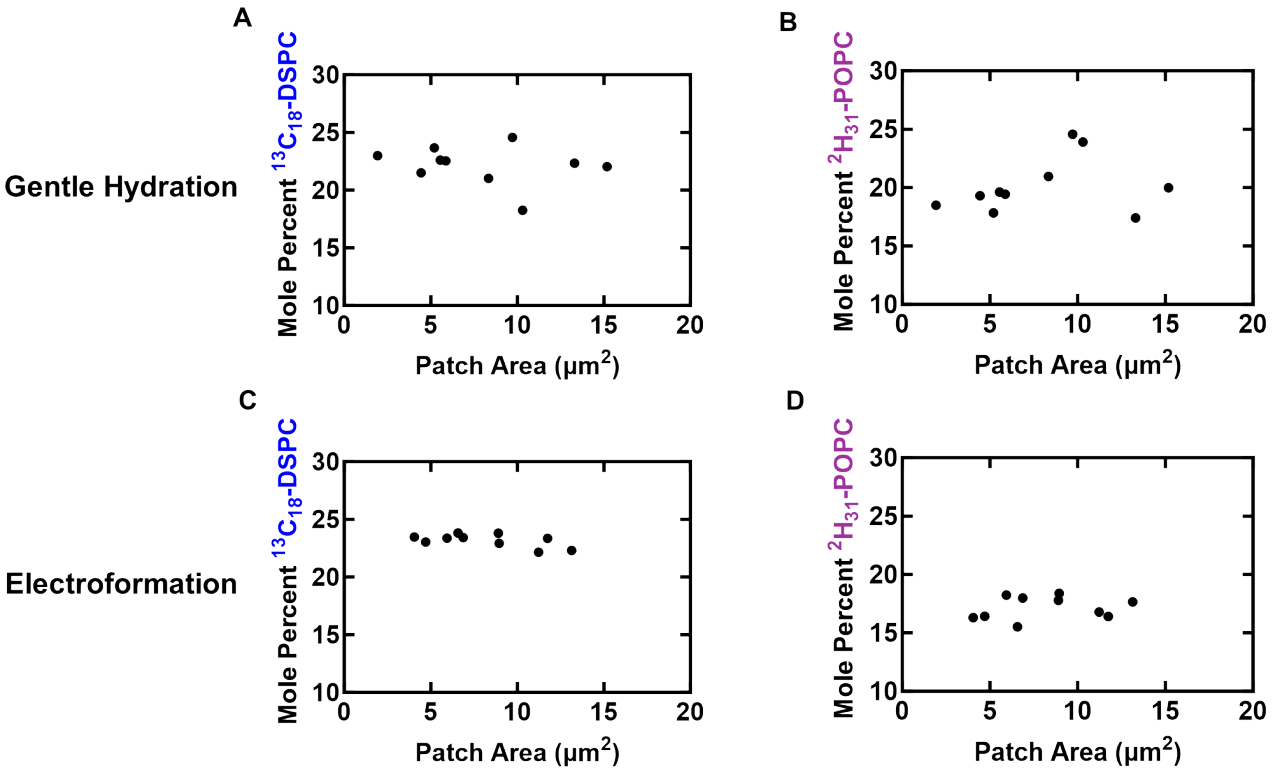

Figure S15. Correlations between patch area and labeled lipid concentrations**.** The relation between observed patch area and concentrations of labeled lipids in a ternary DSPC:$^{13}C_{18}$-DSPC:POPC:$^{2}H_{31}$-POPC:CHOL 20:20:20:20:20 mixture. The association between patch area and $^{13}C_{18}$-DSPC (A) and $^{2}H_{31}$-POPC (B) concentrations for GUVs formed via gentle hydration demonstrates no relation between patch area and labeled lipid concentration. Similar results can be seen in (C) and (D) for GUVs formed via electroformation.

13. Assessing the Extent of GUV Mixing during Patch Formation

Although it is generally assumed that each GUV patch results from the rupture and spreading of a single GUV, it is possible that two or more GUVs may rupture near each other and combine, which would average their two concentrations together. This would result in a decrease in the observed variability in labeled lipid concentrations. To assess the extent to which GUV patches can combine, ternary GUVs with the compositions DSPC:POPC:$^{2}H_{31}$-POPC:CHOL 40:20:20:20 ($^{2}H_{31}$-POPC GUVs) and DSPC:$^{13}C_{18}$-DSPC:POPC:CHOL 20:20:40:20 ($^{13}C_{18}$-DSPC GUVs) were formed via gentle hydration. GUV patches were then prepared on NanoSIMS substrates either using $^{2}H_{31}$-POPC GUVs, $^{13}C_{18}$-DSPC GUVs or a 50:50

(by volume) mixture of the $^{2}H_{31}$-POPC and $^{13}C_{18}$-DSPC GUVs ($^{2}H_{31}$-POPC GUVs + $^{13}C_{18}$-DSPC GUVs). The $^{2}H^{-}/^{13}C^{-}$ ratio was then measured for 15 ($^{2}H_{31}$-POPC GUVs and $^{13}C_{18}$-DSPC GUVs) or 30 ($^{2}H_{31}$-POPC GUVs + $^{13}C_{18}$-DSPC GUVs) patches. The resulting ratios can be seen in Figure S16. Both the $^{2}H_{31}$-POPC and $^{13}C_{18}$-DSPC GUV patches have high and low ratios respectively and are monomodal, as only one labeled lipid is present in each of these GUV samples. For the sample prepared using a mixture of $^{2}H_{31}$-POPC GUVs and $^{13}C_{18}$-DSPC GUVs ($^{2}H_{31}$-POPC GUVs + $^{13}C_{18}$-DSPC GUVs), the resulting ratios have two major clusters, or populations. Each population has a ratio similar to that of the samples prepared using only $^{2}H_{31}$-POPC or $^{13}C_{18}$-DSPC GUVs, suggesting that the majority of the patches are not substantially cross-contaminated with another labeled species. This suggests that the majority of individual GUV patches do not result from the averaging of multiple GUVs. However, a few patches were observed with some level of cross-contamination and have $^{2}H^{-}/^{13}C^{-}$ ratios between the two major populations. These patches contain approximately 3-5 mol % of the non-dominant labeled species, suggesting that some averaging between the $^{13}C_{18}$-DSPC and $^{2}H_{31}$-POPC GUVs occurred in these patches. Additionally, the two dominant populations in the mixed sample appear to be slightly broadened, suggesting that these patches may have some minimal level of contamination from the other label. This may result from debris formed during the freeze-drying process (see section 9 of the supporting information) which may lead to minor contamination (less than 1 mol %) of patches. This merging of GUVs to form single patches has been observed in prior work[5].

It should also be noted that one GUV may lead to the formation of several patches[6]. It cannot be established in this work if different patches resulting from the same parent GUV have different compositions, as these patches cannot be distinguished. As a result, it cannot be determined how this affects the observed variability in GUV patch composition. Given that one GUV may lead to multiple patches, this makes the use of a mixture with nanoscale separation, such as the mixture used here, a better choice for compositional analysis, as GUVs with nanoscale separation are likely less susceptible to large-scale compositional changes during GUV rupture.

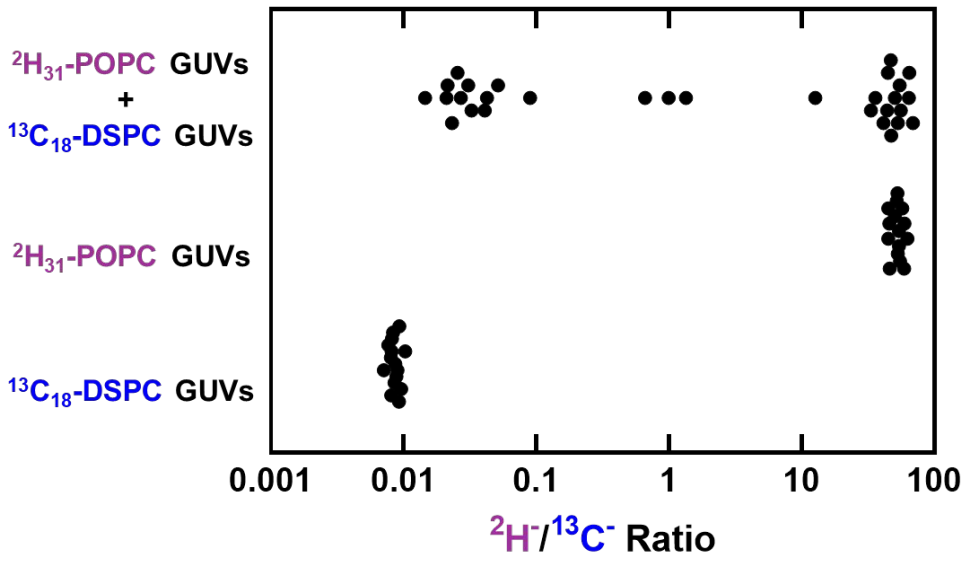

Figure S16. Extent of mixing during GUV patch formation. $^{2}H^{-}/^{13}C^{-}$ Ratios for GUV patches formed with GUVs containing either $^{2}H_{31}$-POPC or $^{13}C_{18}$-DSPC.When GUVs containing only $^{2}H_{31}$-POPC or only $^{13}C_{18}$-DSPC were deposited on NanoSIMS substrates, high and low $^{2}H^{-}/^{13}C^{-}$ ratios were measured respectively. When a mixture of the differently labeled GUVs were deposited on a NanoSIMS substrate, the resulting distribution of ratios is predominantly bimodal, with ratios reflecting that of the GUV patches containing only one labeled lipid.

14. Tracking Cholesterol Concentrations in Triply Labeled Bilayers

As further evidence for the changes in cholesterol concentration seen in Figure 7, triply labeled bilayer patches were formed from GUVs using a master stock with nominal composition 20:20:20:20:20 POPC:^{15}N-POPC:DSPC:$^{13}C_{18}$-DSPC:$^{2}H_{7}$-CHOL. This mixture allows for every lipid component to be tracked. Calibration curves for ^{15}N-POPC and $^{2}H_{7}$-CHOL are shown in Figure S17. As can be seen in Figure S18A, each isotopically labeled species can be visualized and quantified. The average concentration across 8-9 bilayers was measured for patches formed via electroformation or gentle hydration as well as continuous bilayers formed via rupture of SUVs. Figure S18B shows that neither $^{13}C_{18}$-DSPC nor ^{15}N-POPC are significantly different in terms of concentration between the three methods, but the average $^{2}H_{7}$-cholesterol concentration is significantly lower in electroformed GUVs. The ^{15}N-POPC concentration is also significantly higher in GUVs formed by electroformation relative to those formed by gentle hydration ($p = 0.037$). Since electroformed GUVs contain less cholesterol, the concentration of other lipids must be higher, explaining why there is a slight increase in the average ^{15}N-POPC concentration. However, it should be noted that a total of 9 average concentrations were compared (three different labeled species compared between the three different methods), therefore if the required significance level is adjusted to match the number of comparisons using the Bonferroni correction, (α/n, where n = the number of tests conducted),

this difference would no longer be statistically significant. The changes in cholesterol concentration remain statistically significant regardless of whether or not this adjustment is performed.

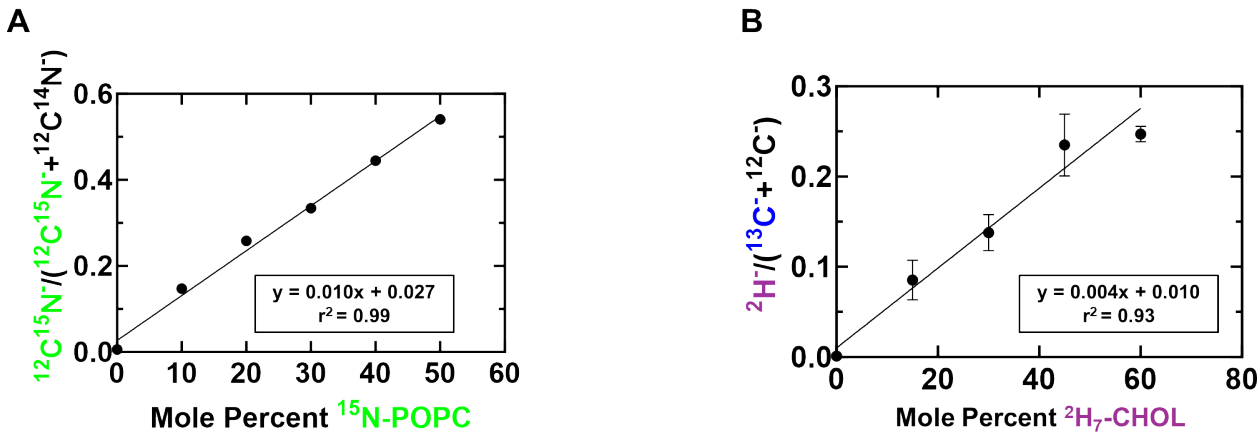

Figure S17. Additional calibration curves. Concentration calibration curves for (A) ^{15}N-POPC and (B) $^{2}H_7$-cholesterol.

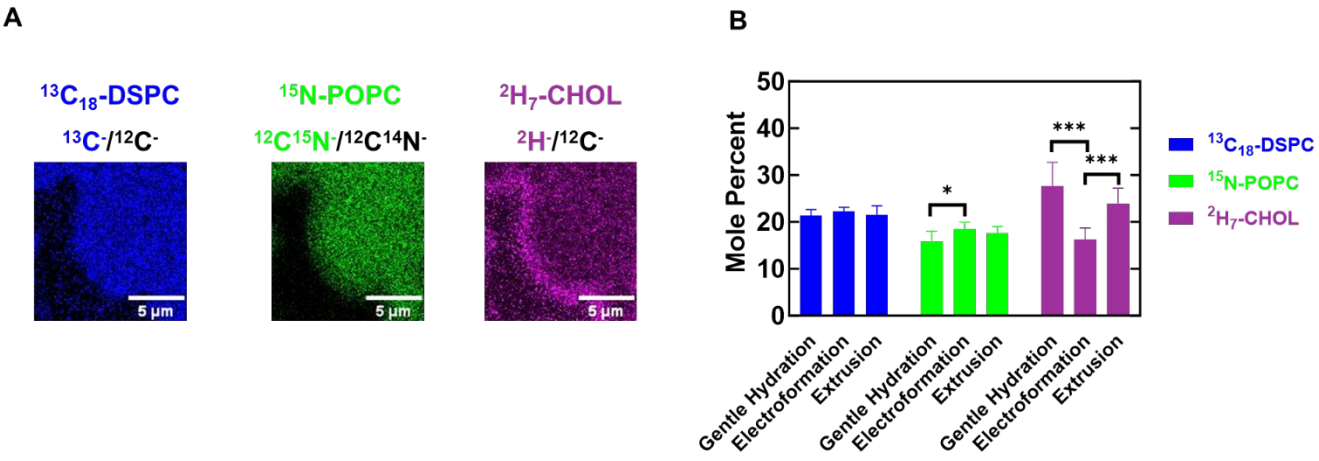

Figure S18. Cholesterol concentrations in triply labeled bilayers. (A) Displays NanoSIMS images of bilayer patches containing $^{13}C_{18}$-DSPC, ^{15}N-POPC and $^{2}H_7$-cholesterol. While both labeled DSPC and POPC are relatively homogenous, the labeled cholesterol displays strong partitioning towards the edge of the bilayer patch. (B) Direct comparison of concentration of labeled lipids and cholesterol in bilayers formed via gentle hydration, electroformation, or through the rupture of SUVs to form continuous bilayers. Only statistically significant changes are marked in the plot. 9 total t-tests were conducted to compare the concentrations of labeled species for each method.

15. Assessing Average $^{2}H_{31}$-POPC Concentration in $^{13}C_{27}$-CHOL Containing Patches

The average concentration of $^{2}H_{31}$-POPC was also measured for the GUV patches analyzed in Figure 7 of the main text. Analysis was conducted both including and excluding edges (same regions of interest as were used in Figure 7 of the main text). Figure S19 shows that regardless of whether edges were included or excluded, the average $^{2}H_{31}$-POPC remained constant between GUV patches formed via electroformation or gentle hydration. It may be expected that the $^{2}H_{31}$-POPC concentration in electroformed GUVs will be higher, given that the lower average cholesterol concentration in these GUVs must lead to higher concentrations of other species; however, there is only a 3-5 mol % decrease in cholesterol concentration in GUVs formed via electroformation. Labeled $^{2}H_{31}$-POPC only makes up 25% of the remaining mixture so only a 1 mol % increase could reasonably be expected in $^{2}H_{31}$-POPC concentration in electroformed GUVs relative to GUVs formed via gentle hydration. Since this is a relatively small change, it is not detectable within the error of the experiment. Additionally, there is a statistically significant increase ($p = 0.0489$) in $^{2}H_{31}$-POPC between analyses including and excluding the edges of bilayer patches formed by gentle hydration (Figure S19). Since the analyses with the edge excluded show a higher average $^{2}H_{31}$-POPC concentration, this can be rationalized by noting that cholesterol appears to be enriched at the edges of bilayers patches, therefore another lipid must have a lower concentration. However, this increase in $^{2}H_{31}$-POPC concentration does not appear to be consistent for both GUVs formed via gentle hydration or electroformation and is not reproduced in replicates (Figure S20B). This suggests that the change in POPC concentrations between the edge and center is minimal within the sensitivity of the experiment.

Given that other GUV patch samples display disagreements between their measured concentrations and the nominal concentrations of their respective stock solutions, these replicates suggest that these differences in cholesterol concentration are reproducible and likely not the result of error in the measurements. However, it is worth noting that there is error in absolute concentration for cholesterol as well, likely due to aforementioned surface contamination, calibration curve accuracy and error in the concentration of lipid stock solutions.

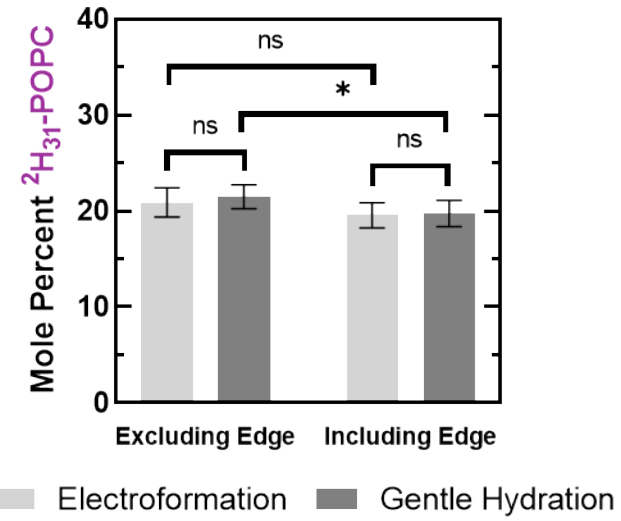

Figure S19. $^{2}H_{31}$-POPC concentrations in GUV patches. Concentrations of $^{2}H_{31}$-POPC measured for the analyses presented in Figure 7 of the main text. GUVs had nominal composition DSPC:POPC:$^{2}H_{31}$-POPC:$^{13}C_{27}$-CHOL 40:20:20:20. Unlike cholesterol concentrations, labeled POPC concentrations do not vary between GUV formation methods regardless of whether or not the data are analyzed either including or excluding the cholesterol-rich edges.

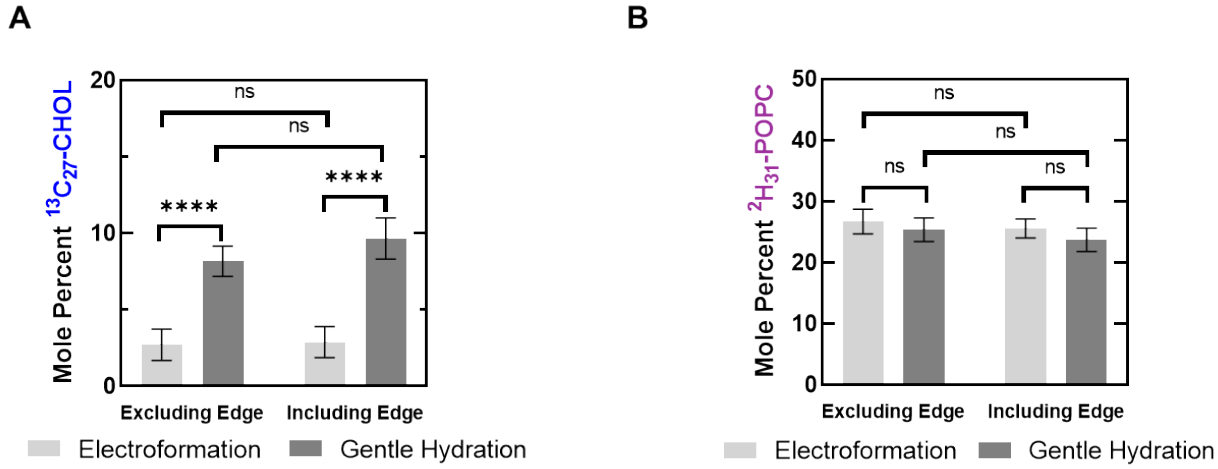

Figure S20. Replicate $^{13}C_{27}$-cholesterol samples. (A) Displays cholesterol concentrations for GUV patches formed by either electroformation or gentle hydration. Bilayer patches were analyzed either including or excluding cholesterol-rich edges. (B) $^{2}H_{31}$-POPC concentrations are not significantly different between GUV patches formed via gentle hydration and electroformation.

16. Tabulated Raw GUV Composition Data

The tables below record $^{2}H^{-}/^{13}C^{-}$ ratios, as well as labeled lipid compositions for all figures in the main text and supporting information. Ratios and compositions are reported to two decimal places, although it should be noted that the second decimal place is presumably less accurate, however for the purposes of reporting the data, it has been left in. Tables have been organized according to the figures they correspond to (as denoted in the table title) and are listed in order of appearance.

Tables S1A-C. Raw data from Figures 4A, 5B and 5C of the main text.

A

Mole Percent $^{2}H_{31}$-POPC Gentle Hydration (Figure 6A)	
Pure POPC	Ternary Mixture
23.95	25.49
23.08	20.54
22.07	21.90
23.13	22.73
21.00	24.24
20.74	19.23
20.61	21.71
22.56	23.90
22.89	25.96
23.21	24.93
25.63	23.52
24.01	15.64
20.47	23.76
25.22	27.59
21.68	23.07
24.03	25.63
23.17	25.11
25.02	14.78
21.63	22.71
22.07	24.37
23.23	31.22
21.20	31.99
23.47	23.03
23.86	21.98
22.16	18.49
22.57	22.01
24.41	26.61
22.35	28.09
23.20	23.34
22.89	24.86

B

Mole Percent $^{2}H_{31}$-POPC Electroformation (Figure 6B)	
Pure POPC	Ternary Mixture
18.86	23.55
20.81	24.33
19.10	25.73
21.64	24.33
20.19	23.46
22.86	27.27
20.33	26.30
19.26	24.45
14.80	22.49
18.53	27.84
18.28	28.12
19.75	23.74
19.36	25.51
24.80	26.38
21.52	27.37
19.50	26.43
15.93	28.14
18.84	25.90
25.57	24.52
24.58	22.41
22.71	24.62
20.07	26.80
18.21	25.26
19.56	25.77
19.73	24.09
20.48	25.23
23.72	24.44
23.94	23.53
22.32	24.29
20.81	26.62

Tables S2A-B. Raw data from Figure 6A and B of the main text.

A

^{2}H-/^{13}C- Ratios (Figure 4A)		
Gentle Hydration	Electroformation	Continuous Bilayer
8.51	6.80	7.03
6.38	7.39	7.34
6.67	6.56	6.38
6.82	7.34	7.05
7.43	7.28	8.55
5.21	7.93	7.42
6.92	7.13	8.36
7.88	6.49	8.23
8.95	4.73	7.30
8.47	5.99	7.57
7.61	6.09	8.14
4.32	6.63	7.67
7.83	6.40	7.33
9.24	8.85	7.99
7.34	7.43	8.98
8.53	6.77	6.25
8.70	5.09	6.83
4.43	6.42	8.38
7.30	9.60	7.67
8.55	8.91	8.54
10.77	7.85	7.66
11.02	7.02	7.34
7.43	5.86	6.18
6.82	6.55	7.79
5.52	6.87	8.59
6.99	6.98	7.65
9.00	8.09	7.70
9.73	8.30	7.99
7.45	7.47	8.55
8.54	6.78	7.38

B

Mole Percent $^{13}C_{18}$-DSPC (Figure 5B)	
Gentle Hydration	Electroformation
24.61	22.92
27.03	23.18
27.54	24.22
27.94	24.40
27.19	22.84
31.59	23.70
26.17	23.57
25.05	24.73
23.71	26.73
24.16	25.97
25.63	25.16
31.31	24.81
25.07	25.28
24.45	22.87
26.13	23.90
24.72	23.90
23.61	26.62
28.75	24.44
25.84	21.52
23.33	22.45
23.51	23.82
23.54	23.66
25.73	26.17
26.94	24.90
28.42	23.81
26.26	24.33
24.23	24.11
23.49	23.65
26.03	24.71
23.86	25.56

C

Mole Percent $^{2}H_{31}$-POPC (Figure 5C)		
Gentle Hydration	Electroformation	Pure POPC Monolayer
25.49	18.86	23.29
20.54	20.81	22.78
21.90	19.10	21.31
22.73	21.64	21.83
24.24	20.19	25.14
19.23	22.86	24.47
21.71	20.33	23.12
23.90	19.26	23.59
25.96	14.80	22.33
24.93	18.53	22.18
23.52	18.28	24.33
15.64	19.75	23.62
23.76	19.36	22.04
27.59	24.80	22.89
23.07	21.52	21.90
25.63	19.50	22.57
25.11	15.93	20.83
14.78	18.84	21.02
22.71	25.57	23.78
24.37	24.58	23.79
31.22	22.71	22.40
31.99	20.07	22.44
23.03	18.21	19.87
21.98	19.56	20.99
18.49	19.73	20.17
22.01	20.48	19.94
26.61	23.72	20.93
28.09	23.94	21.23
23.34	22.32	21.11
24.86	20.81	20.68

Tables S3 A-C. Raw data from Figure S4 of the supporting information.

A

^{2}H-/^{13}C- Ratios Replicate Samples (Figure S4A)	
Gentle Hydration	Electroformation
6.29	8.63
9.07	8.72
4.96	7.21
10.20	8.61
4.91	6.53
6.56	8.95
6.92	8.50
7.97	8.19
7.26	8.89
5.63	8.25
7.89	8.54
5.30	10.27
6.30	8.34
6.99	8.15
5.33	7.90
6.49	7.81
7.29	8.49
5.90	8.94
4.86	7.75
8.33	8.31
7.07	9.26
7.71	10.22
4.13	9.87
7.33	9.17
5.04	9.21
6.89	8.90
8.41	9.83
8.95	7.50
8.21	7.83
8.37	6.67

B

Mole Percent $^{13}C_{18}$-DSPC Replicate Samples (Figure S4B)	
Gentle Hydration	Electroformation
15.92	22.43
19.51	22.87
12.83	19.59
23.62	21.69
13.70	18.73
16.55	19.36
17.05	21.39
19.20	21.43
17.15	22.69
13.92	22.01
19.04	22.32
12.33	26.40
15.60	22.61
17.35	19.69
13.51	21.80
16.50	21.29
18.14	23.70
16.43	25.04
13.19	22.56
22.55	23.44
19.55	25.43
20.63	27.32
12.65	26.61
18.79	25.76
14.60	24.93
19.34	24.31
21.96	25.95
22.81	21.60
21.89	22.33
21.65	19.87

C

Mole Percent $^{2}H_{31}$-POPC Replicate Samples (Figure S4C)	
Gentle Hydration	Electroformation
20.87	21.05
17.00	21.27
21.79	22.33
18.34	20.33
23.66	23.86
20.74	17.11
20.12	20.33
19.45	21.28
19.14	20.59
20.54	21.73
19.48	21.20
19.31	20.61
20.38	22.08
20.29	19.48
21.20	22.59
20.94	22.32
20.27	22.81
23.24	22.82
22.97	23.98
22.06	23.09
22.81	22.30
21.87	21.55
26.48	21.78
20.93	22.88
24.54	21.95
23.21	22.21
21.19	21.28
20.56	23.74
21.72	23.44
20.98	24.78

Tables S4 A-F. Raw data from Figure S7 of the supporting information.

A

^{2}H-/^{13}C- Ratios Gentle Hydration (Figure S7A)	
Full Patch	Fixed Area
8.51	9.73
6.38	6.40
6.67	7.34
6.82	6.70
7.43	7.59
5.21	6.41
6.92	7.43
7.88	7.31
8.95	7.51
8.47	9.91
7.61	8.84
4.32	3.78
7.83	7.75
9.24	11.85
7.34	8.15
8.53	8.72
8.70	9.36
4.43	4.47
7.30	8.37
8.55	8.60
10.77	10.87
11.02	12.09
7.43	8.62
6.82	5.29
5.52	5.24
6.99	7.97
9.00	9.69
9.73	10.87
7.45	8.43
8.54	8.24

B

Mole Percent $^{13}C_{18}$-DSPC Gentle Hydration (Figure S7B)	
Full Patch	Fixed Area
24.61	23.03
27.03	26.85
27.54	26.50
27.94	28.05
27.19	26.98
31.59	29.00
26.17	25.25
25.05	25.75
23.71	26.65
24.16	22.67
25.63	23.82
31.31	32.03
25.07	26.54
24.45	21.12
26.13	24.96
24.72	24.72
23.61	22.07
28.75	28.61
25.84	23.86
23.33	23.29
23.51	22.14
23.54	22.10
25.73	23.99
26.94	30.58
28.42	27.97
26.26	24.92
24.23	23.21
23.49	22.55
26.03	23.85
23.86	24.40

C

Mole Percent $^{2}H_{31}$-POPC Gentle Hydration (Figure S7C)	
Full Patch	Fixed Area
25.49	27.56
20.54	20.50
21.90	23.37
22.73	22.40
24.24	24.61
19.23	22.05
21.71	22.64
23.90	22.66
25.96	24.08
24.93	27.71
23.52	25.74
15.64	13.85
23.76	24.76
27.59	31.28
23.07	24.67
25.63	26.22
25.11	25.49
14.78	14.84
22.71	24.34
24.37	24.51
31.22	29.85
31.99	33.26
23.03	25.23
21.98	18.96
18.49	17.24
22.01	24.08
26.61	27.66
28.09	30.35
23.34	24.50
24.86	24.44

D

^{2}H-/^{13}C- Ratios Electroformation (Figure S7D)	
Full Patch	Fixed Area
6.80	6.90
7.39	7.95
6.56	8.49
7.34	7.70
7.28	9.48
7.93	8.15
7.13	8.60
6.49	8.51
4.73	5.83
5.99	7.28
6.09	7.34
6.63	8.79
6.40	7.40
8.85	9.33
7.43	7.84
6.77	9.77
5.09	6.77
6.42	8.15
9.60	9.59
8.91	9.56
7.85	9.27
7.02	7.23
5.86	6.24
6.55	7.21
6.87	5.74
6.98	6.90
8.09	7.57
8.30	9.31
7.47	8.57
6.78	7.98

E

Mole Percent $^{13}C_{18}$-DSPC Electroformation (Figure S7E)	
Full Patch	Fixed Area
22.92	23.20
23.18	22.57
24.22	22.56
24.40	24.21
22.84	21.04
23.70	23.48
23.57	22.44
24.73	22.27
26.73	25.75
25.97	24.78
25.16	23.81
24.81	22.82
25.28	24.33
22.87	22.74
23.90	23.54
23.90	20.22
26.62	24.09
24.44	22.47
21.52	21.63
22.45	21.72
23.82	22.67
23.66	24.71
26.17	24.96
24.90	24.19
23.81	25.84
24.33	24.76
24.11	25.49
23.65	23.29
24.71	24.18
25.56	23.93

F

Mole Percent $^{2}H_{31}$-POPC Electroformation (Figure S7F)	
Full Patch	Fixed Area
18.86	19.37
20.81	21.92
19.10	23.48
21.64	22.62
20.19	24.74
22.86	23.31
20.33	23.67
19.26	23.25
14.80	17.85
18.53	21.76
18.28	21.15
19.75	24.58
19.36	21.78
24.80	26.09
21.52	22.46
19.50	24.63
15.93	19.64
18.84	22.39
25.57	25.65
24.58	25.66
22.71	25.83
20.07	21.55
18.21	18.64
19.56	21.09
19.73	17.62
20.48	20.57
23.72	23.28
23.94	26.59
22.32	25.25
20.81	23.20

Table S5 A-C. Raw data from Figure S8 of the supporting information.

A

$^{2}H^{-}/^{13}C^{-}$ Ratios Fixed Area (Figure S8A)	
Gentle Hydration	Electroformation
9.73	6.90
6.40	7.95
7.34	8.49
6.70	7.70
7.59	9.48
6.41	8.15
7.43	8.60
7.31	8.51
7.51	5.83
9.91	7.28
8.84	7.34
3.78	8.79
7.75	7.40
11.85	9.33
8.15	7.84
8.72	9.77
9.36	6.77
4.47	8.15
8.37	9.59
8.60	9.56
10.87	9.27
12.09	7.23
8.62	6.24
5.29	7.21
5.24	5.74
7.97	6.90
9.69	7.57
10.87	9.31
8.43	8.57
8.24	7.98

B

Mole Percent $^{13}C_{18}$-DSPC Fixed Area (Figure S8B)	
Gentle Hydration	Electroformation
23.03	23.20
26.85	22.57
26.50	22.56
28.05	24.21
26.98	21.04
29.00	23.48
25.25	22.44
25.75	22.27
26.65	25.75
22.67	24.78
23.82	23.81
32.03	22.82
26.54	24.33
21.12	22.74
24.96	23.54
24.72	20.22
22.07	24.09
28.61	22.47
23.86	21.63
23.29	21.72
22.14	22.67
22.10	24.71
23.99	24.96
30.58	24.19
27.97	25.84
24.92	24.76
23.21	25.49
22.55	23.29
23.85	24.18
24.40	23.93

C

Mole Percent $^{2}H_{31}$-POPC Fixed Area (Figure S8C)	
Gentle Hydration	Electroformation
27.56	19.37
20.50	21.92
23.37	23.48
22.40	22.62
24.61	24.74
22.05	23.31
22.64	23.67
22.66	23.25
24.08	17.85
27.71	21.76
25.74	21.15
13.85	24.58
24.76	21.78
31.28	26.09
24.67	22.46
26.22	24.63
25.49	19.64
14.84	22.39
24.34	25.65
24.51	25.66
29.85	25.83
33.26	21.55
25.23	18.64
18.96	21.09
17.24	17.62
24.08	20.57
27.66	23.28
30.35	26.59
24.50	25.25
24.44	23.20

Table S6 A-C. Raw data from Figures S9 and S10 of the supporting information.

A

Mole Percent $^{13}C_{18}$ Lipid Gentle Hydration (Figure S9A)	
Pure POPC ($^{13}C_{18}$-POPC)	Ternary Mixture ($^{13}C_{18}$-DSPC)
20.74	24.61
20.94	27.03
20.65	27.54
20.82	27.94
21.97	27.19
21.49	31.59
22.03	26.17
21.54	25.05
22.24	23.71
21.93	24.16
22.06	25.63
22.30	31.31
21.57	25.07
22.04	24.45
22.06	26.13
21.62	24.72
20.98	23.61
23.30	28.75
22.97	25.84
22.06	23.33
21.53	23.51
21.53	23.54
21.67	25.73
22.65	26.94
22.34	28.42
22.29	26.26
22.42	24.23
21.94	23.49
21.49	26.03
22.06	23.86

B

Mole Percent $^{13}C_{18}$ Lipid Electroformation (Figure S9B)	
Pure POPC ($^{13}C_{18}$-POPC)	Ternary Mixture ($^{13}C_{18}$-DSPC)
20.41	22.92
22.09	23.18
22.31	24.22
22.51	24.40
22.43	22.84
22.06	23.70
22.12	23.57
22.31	24.73
21.65	26.73
22.70	25.97
22.27	25.16
22.14	24.81
22.79	25.28
22.20	22.87
21.75	23.90
22.01	23.90
22.57	26.62
22.89	24.44
22.90	21.52
22.48	22.45
22.16	23.82
21.86	23.66
22.48	26.17
22.59	24.90
23.16	23.81
22.66	24.33
23.14	24.11
23.28	23.65
22.83	24.71
22.97	25.56

C

Mole Percent $^{2}H_{31}$-POPC Pure POPC (Figure S10A)	
Gentle Hydration	Electroformation
23.55	23.95
24.33	23.08
25.73	22.07
24.33	23.13
23.46	21.00
27.27	20.74
26.30	20.61
24.45	22.56
22.49	22.89
27.84	23.21
28.12	25.63
23.74	24.01
25.51	20.47
26.38	25.22
27.37	21.68
26.43	24.03
28.14	23.17
25.90	25.02
24.52	21.63
22.41	22.07
24.62	23.23
26.80	21.20
25.26	23.47
25.77	23.86
24.09	22.16
25.23	22.57
24.44	24.41
23.53	22.35
24.29	23.20
26.62	22.89

17. Dot Plot representations of GUV Composition Distributions

All GUV compositions are re-plotted below as dot plots without the overlayed gaussian distribution. Dot plots are presented in the order in which they appear in the main text and supporting information. Red lines denote the nominal concentration of labeled lipid present in the master stock and all significance is determined by F-test, as described in the main text.

A

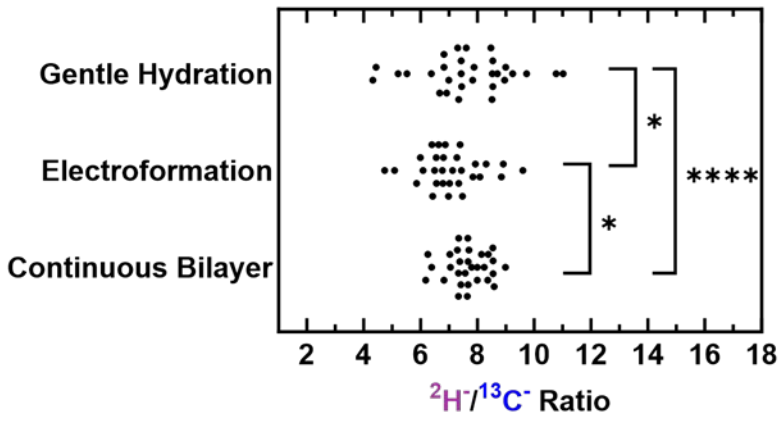

B

Method	$^{2}H^{-}/^{13}C^{-}$ Standard Deviation
Gentle Hydration	1.6
Electroformation	1.1
Continuous Bilayer	0.7

Figure S21. (A) Depicts the dot plot representation of the data in Figure 4A of the main text. (B) corresponding table of calculated standard deviations. As in the main text, significance was determined via F-test. For this and subsequent plots, each point represents a measurement made on a single GUV patch or corral containing an SLB. Thirty bilayers were examined for each sample. For this and all subsequent plots, * $p \leq 0.05$, ** $p \leq 0.01$, *** $p \leq 0.001$, **** $p \leq 0.0001$.

A

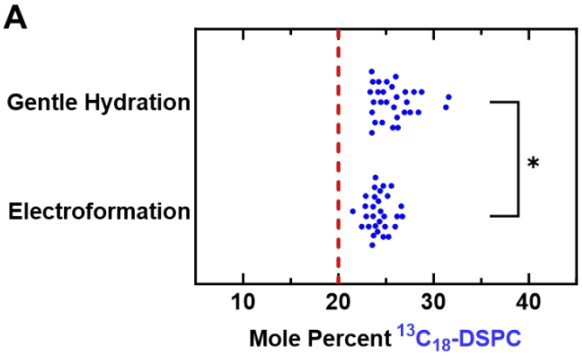

B

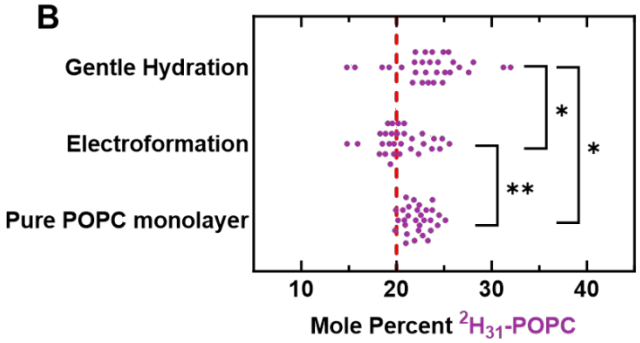

C

Method	[$^{2}H_{31}$-POPC] Standard Deviation	[$^{13}C_{18}$-DSPC] Standard Deviation
Gentle Hydration	3.7	2.2
Electroformation	2.5	1.2
Pure POPC monolayer	1.4	n/a

Figure S22. (A) and (B) depict the dot plot representations of the data in Figures 5B and 5C of the main text. (C) Displays the corresponding standard deviations.

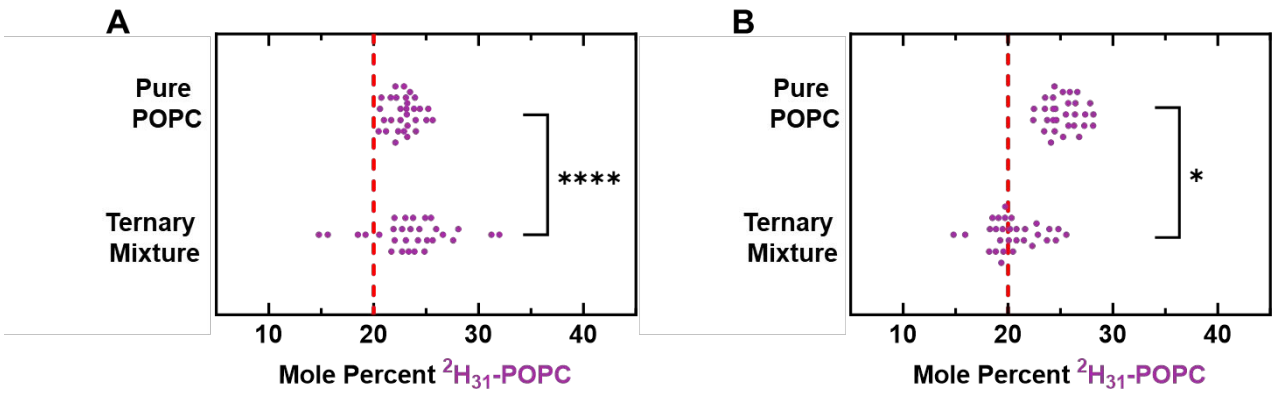

C

Method	[$^{2}H_{31}$-POPC] Standard Deviation	
	Pure POPC	Ternary Mixture
Gentle Hydration	1.4	3.7
Electroformation	1.6	2.5

Figure S23. (A) and (B) depict the dot plot representations of the data in Figures 6A and 6B of the main text. (C) Displays the corresponding standard deviations.

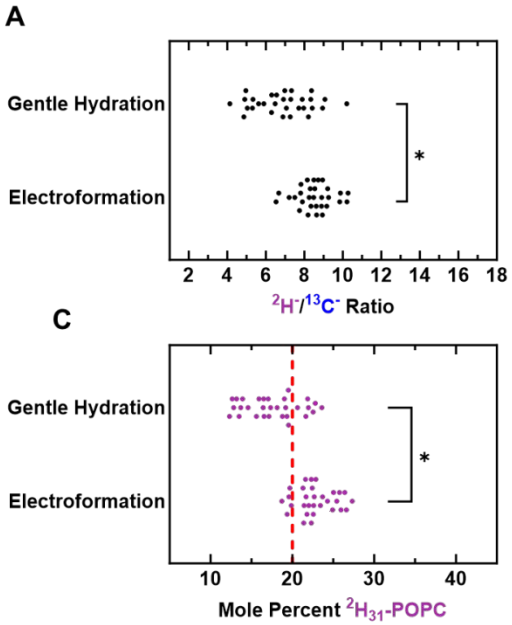

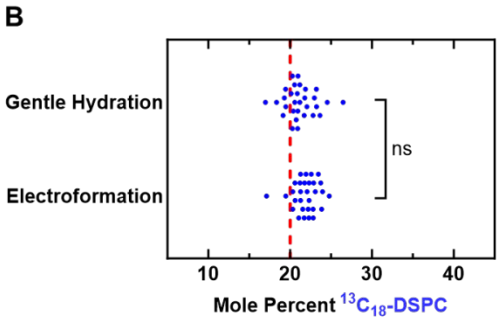

D

Method	$^{2}H^{-}/^{13}C^{-}$ Ratio Standard Deviation	[$^{13}C_{18}$-DSPC] Standard Deviation	[$^{2}H_{31}$-POPC] Standard Deviation
Gentle Hydration	1.5	1.9	3.4
Electroformation	0.9	1.5	2.3

Figure S24. (A-C) Depict the dot plot representations of the data in Figure S4A-C of the supporting information. (D) Displays the corresponding standard deviations.

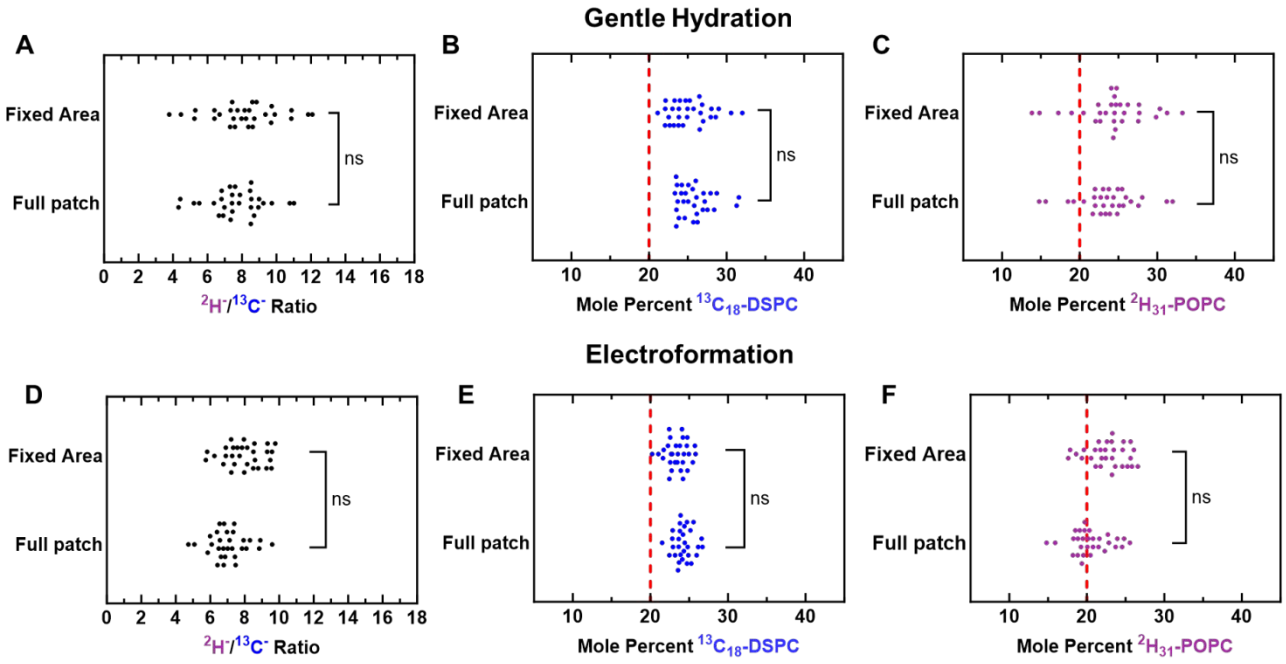

G

Gentle Hydration			
Analysis Method	$^{2}H^{-}/^{13}C^{-}$ Ratio Standard Deviation	[$^{13}C_{18}$-DSPC] Standard Deviation	[$^{2}H_{31}$-POPC] Standard Deviation
Fixed Area	2.0	2.7	4.3
Full Patch	1.6	2.2	3.7

H

Electroformation			
Analysis Method	$^{2}H^{-}/^{13}C^{-}$ Ratio Standard Deviation	[$^{13}C_{18}$-DSPC] Standard Deviation	[$^{2}H_{31}$-POPC] Standard Deviation
Fixed Area	1.1	1.4	2.5
Full Patch	1.1	1.2	2.6

Figure S25. (A-F) Depict the dot plot representations of the data in Figure S7A-F of the supporting information. (G-H) Display the corresponding standard deviations.

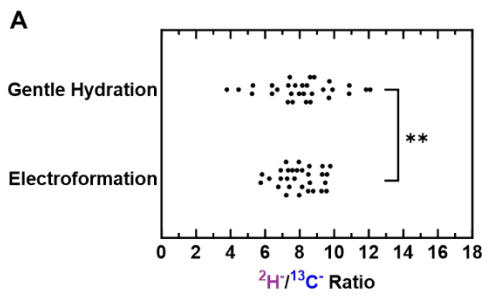

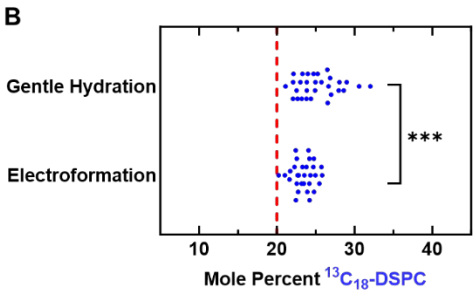

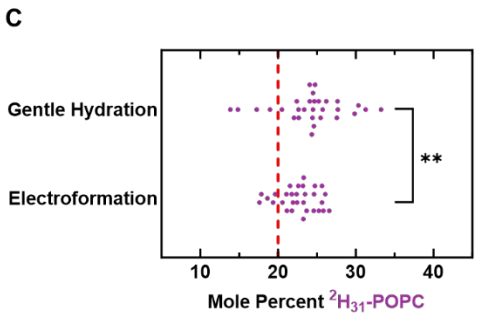

D

Method	$^{2}H^{-}/^{13}C^{-}$ Ratio Standard Deviation	[$^{13}C_{18}$-DSPC] Standard Deviation	[$^{2}H_{31}$-POPC] Standard Deviation
Gentle Hydration	2.0	2.7	4.3
Electroformation	1.1	1.4	2.5

Figure S26. (A-C) Depict the dot plot representations of the data in Figure S8A-C. (D) Displays the corresponding standard deviations.

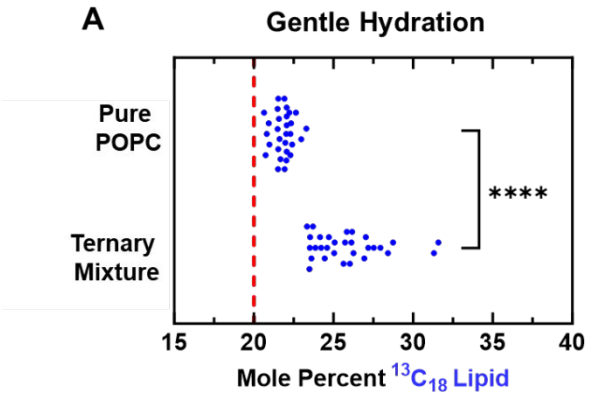

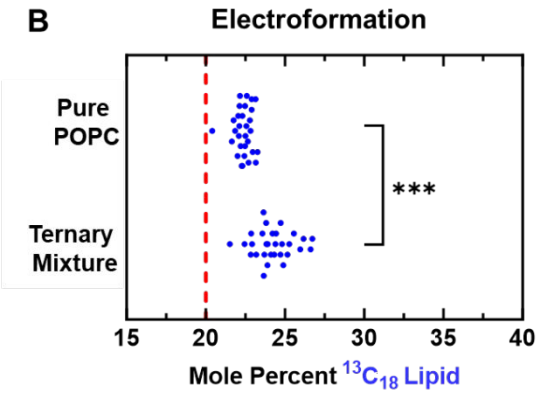

C

Method	[$^{13}C_{18}$ Lipid] Standard Deviation	
	Pure POPC	Ternary Mixture
Gentle Hydration	0.6	2.2
Electroformation	0.6	1.2

Figure S27. (A) and (B) depict the dot plot representation of the data in Figure S9A and S9B of the supporting information. (C) Displays the corresponding standard deviations.

A

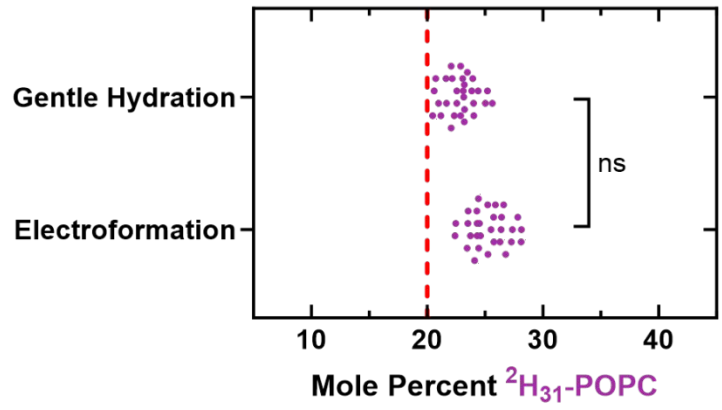

B

Method	[$^{2}H_{31}$-POPC] Standard Deviation
Gentle Hydration	1.4
Electroformation	1.6

Figure S28. (A) Depicts the dot plot representation of the data in Figure S10 of the supporting information. (B) Displays the corresponding standard deviations.

References

(1) Konyakhina, T. M.; Wu, J.; Mastroianni, J. D.; Heberle, F. A.; Feigenson, G. W. Phase Diagram of a 4-Component Lipid Mixture: DSPC/DOPC/POPC/Chol. *Biochim. Biophys. Acta BBA - Biomembr.* **2013**, *1828* (9), 2204–2214. https://doi.org/10.1016/j.bbamem.2013.05.020.

(2) Moss, F. R.; Boxer, S. G. Atomic Recombination in Dynamic Secondary Ion Mass Spectrometry Probes Distance in Lipid Assemblies: A Nanometer Chemical Ruler. *J. Am. Chem. Soc.* **2016**, *138* (51), 16737–16744. https://doi.org/10.1021/jacs.6b10655.

(3) Grusky, D. S.; Moss, F. R.; Boxer, S. G. Recombination between ^{13}C and ^{2}H to Form Acetylide ($^{13}C_2{}^{2}H^-$) Probes Nanoscale Interactions in Lipid Bilayers via Dynamic Secondary Ion Mass Spectrometry: Cholesterol and GM_1 Clustering. *Anal. Chem.* **2022**, *94* (27), 9750–9757. https://doi.org/10.1021/acs.analchem.2c01336.

(4) Legent, G.; Delaune, A.; Norris, V.; Delcorte, A.; Gibouin, D.; Lefebvre, F.; Misevic, G.; Thellier, M.; Ripoll, C. Method for Macromolecular Colocalization Using Atomic Recombination in Dynamic SIMS. *J. Phys. Chem. B* **2008**, *112* (17), 5534–5546. https://doi.org/10.1021/jp7100489.

(5) Goodband, R. J.; Bain, C. D.; Staykova, M. Comparative Study of Lipid- and Polymer-Supported Membranes Obtained by Vesicle Fusion. *Langmuir* **2022**, *38* (18), 5674–5681. https://doi.org/10.1021/acs.langmuir.2c00266.

(6) Ngassam, V. N.; Su, W.-C.; Gettel, D. L.; Deng, Y.; Yang, Z.; Wang-Tomic, N.; Sharma, V. P.; Purushothaman, S.; Parikh, A. N. Recurrent Dynamics of Rupture Transitions of Giant Lipid Vesicles at Solid Surfaces. *Biophys. J.* **2021**, *120* (4), 586–597. https://doi.org/10.1016/j.bpj.2021.01.006.